Dear Author,

Here are the proofs of your article.

- You can submit your corrections **online**, via **e-mail** or by **fax**.
- For **online** submission please insert your corrections in the online correction form. Always indicate the line number to which the correction refers.
- You can also insert your corrections in the proof PDF and **email** the annotated PDF.
- For fax submission, please ensure that your corrections are clearly legible. Use a fine black pen and write the correction in the margin, not too close to the edge of the page.
- Remember to note the **journal title**, **article number**, and **your name** when sending your response via e-mail or fax.
- **Check** the metadata sheet to make sure that the header information, especially author names and the corresponding affiliations are correctly shown.
- **Check** the questions that may have arisen during copy editing and insert your answers/ corrections.
- **Check** that the text is complete and that all figures, tables and their legends are included. Also check the accuracy of special characters, equations, and electronic supplementary material if applicable. If necessary refer to the *Edited manuscript*.
- The publication of inaccurate data such as dosages and units can have serious consequences. Please take particular care that all such details are correct.
- Please **do not** make changes that involve only matters of style. We have generally introduced forms that follow the journal's style.
  Substantial changes in content, e.g., new results, corrected values, title and authorship are not allowed without the approval of the responsible editor. In such a case, please contact the Editorial Office and return his/her consent together with the proof.
- If we do not receive your corrections **within 48 hours**, we will send you a reminder.
- Your article will be published **Online First** approximately one week after receipt of your corrected proofs. This is the **official first publication** citable with the DOI. **Further changes are, therefore, not possible.**
- The **printed version** will follow in a forthcoming issue.

Please note

After online publication, subscribers (personal/institutional) to this journal will have access to the complete article via the DOI using the URL: http://dx.doi.org/[DOI].
If you would like to know when your article has been published online, take advantage of our free alert service. For registration and further information go to: http://www.link.springer.com.

Due to the electronic nature of the procedure, the manuscript and the original figures will only be returned to you on special request. When you return your corrections, please inform us if you would like to have these documents returned.

Metadata of the article that will be visualized in OnlineFirst

ArticleTitle	Near-Fault Broadband Ground Motion Simulation Applications at the Central Ionian Islands, Greece	
Article Sub-Title		
Article CopyRight	The Author(s), under exclusive licence to Springer Nature Switzerland AG (This will be the copyright line in the final PDF)	
Journal Name	Pure and Applied Geophysics	
Corresponding Author	Family Name	**Bonatis**
	Particle	
	Given Name	**Pavlos**
	Suffix	
	Division	Geophysics Department
	Organization	Aristotle University of Thessaloniki
	Address	54124, Thessaloniki, Greece
	Phone	
	Fax	
	Email	mponatis@geo.auth.gr
	URL	
	ORCID	http://orcid.org/0000-0002-4742-9352
Author	Family Name	**Akinci**
	Particle	
	Given Name	**Aybige**
	Suffix	
	Division	
	Organization	Istituto Nazionale di Geofisica e Vulcanologia
	Address	Via di Vigna Murata 605, 00143, Rome, Italy
	Phone	
	Fax	
	Email	aybige.akinci@ingv.it
	URL	
	ORCID	
Author	Family Name	**Karakostas**
	Particle	
	Given Name	**Vasileios**
	Suffix	
	Division	Geophysics Department
	Organization	Aristotle University of Thessaloniki
	Address	54124, Thessaloniki, Greece
	Phone	
	Fax	
	Email	vkarak@geo.auth.gr
	URL	

	ORCID	
Author	Family Name	**Papadimitriou**
	Particle	
	Given Name	**Eleftheria**
	Suffix	
	Division	Geophysics Department
	Organization	Aristotle University of Thessaloniki
	Address	54124, Thessaloniki, Greece
	Phone	
	Fax	
	Email	ritsa@geo.auth.gr
	URL	
	ORCID	
Author	Family Name	**Kaviris**
	Particle	
	Given Name	**George**
	Suffix	
	Division	Department of Geophysics and Geothermics
	Organization	National and Kapodistrian University of Athens
	Address	Panepistimiopolis, 15784, Zografou, Greece
	Phone	
	Fax	
	Email	gkaviris@geol.uoa.gr
	URL	
	ORCID	

Schedule	Received	21 October 2020
	Revised	8 July 2021
	Accepted	11 July 2021

Abstract	Physics-based broadband ground-motion simulations are generated for the strong mainshocks that occurred in the region of the Central Ionian Islands, on 26th January 2014 in Kefalonia (M_w6.1) and 17th November 2015 in Lefkas (M_w6.5). The study area is associated with frequent strong earthquakes both in the historical and instrumental era. During the last decades the network of strong-motion accelerographs in the area has been densified, and thus provided an adequate number of strong ground motion records as a means to better examine the related ground motion characteristics. In the present study, broadband ground motions for the two case studies are simulated both at selected sites and at a dense grid of points covering the affected areas. The low-frequency part of the synthetics is computed using a discrete wavenumber finite element method by convolving Green's functions with a kinematic slip model in the frequency domain. A stochastic finite fault model approach based on a dynamic corner frequency is considered to calculate the ground motions for the higher frequencies. The broadband synthetic time series are generated after merging the results obtained from the two separate techniques, by performing a weighted summation at intermediate frequencies. The simulated values are validated by comparison with both recorded Peak Ground Acceleration (PGA) and Peak Ground Velocity (PGV) values and the estimated ones by using widely accepted Ground Motion Prediction Equations (GMPEs). Our results indicate that both the spatial distribution and the amplification pattern of the simulated ground motions, in the near-field, in terms of PGA and PGV are highly influenced by the slip heterogeneity and the maximum slip patches within the seismic source.

Keywords (separated by '-')	Strong ground motion - near-source ground motion - stochastic finite-fault method - discrete wavenumber method - Ionian Islands

Footnote Information **Supplementary Information** The online version contains supplementary material available at https://doi.org/10.1007/s00024-021-02825-9.

Pure Appl. Geophys.

https://doi.org/10.1007/s00024-021-02825-9

Pure and Applied Geophysics

Near-Fault Broadband Ground Motion Simulation Applications at the Central Ionian Islands, Greece

Pavlos Bonatis,[1] Aybige Akinci,[2] Vasileios Karakostas,[1] Eleftheria Papadimitriou,[1] and George Kaviris[3]

Abstract—Physics-based broadband ground-motion simulations are generated for the strong mainshocks that occurred in the region of the Central Ionian Islands, on 26th January 2014 in Kefalonia (M_w6.1) and 17th November 2015 in Lefkas (M_w6.5). The study area is associated with frequent strong earthquakes both in the historical and instrumental era. During the last decades the network of strong-motion accelerographs in the area has been densified, and thus provided an adequate number of strong ground motion records as a means to better examine the related ground motion characteristics. In the present study, broadband ground motions for the two case studies are simulated both at selected sites and at a dense grid of points covering the affected areas. The low-frequency part of the synthetics is computed using a discrete wavenumber finite element method by convolving Green's functions with a kinematic slip model in the frequency domain. A stochastic finite fault model approach based on a dynamic corner frequency is considered to calculate the ground motions for the higher frequencies. The broadband synthetic time series are generated after merging the results obtained from the two separate techniques, by performing a weighted summation at intermediate frequencies. The simulated values are validated by comparison with both recorded Peak Ground Acceleration (PGA) and Peak Ground Velocity (PGV) values and the estimated ones by using widely accepted Ground Motion Prediction Equations (GMPEs). Our results indicate that both the spatial distribution and the amplification pattern of the simulated ground motions, in the near-field, in terms of PGA and PGV are highly influenced by the slip heterogeneity and the maximum slip patches within the seismic source.

Keywords: Strong ground motion, near-source ground motion, stochastic finite-fault method, discrete wavenumber method, Ionian Islands.

1. Introduction

Greece is the most seismically active region in the Mediterranean and among the most active worldwide (Makropoulos et al., 2012; Papazachos & Papazachou, 2003). The Central Ionian Islands area exhibits the highest seismic moment rate in Greece, with the frequent occurrence of strong ($M > 6.0$) destructive earthquakes causing loss of human life, damage to buildings and economic losses. The area constitutes an active boundary per se, connecting the oceanic subduction to the south (Papazachos & Comninakis, 1970) with the continental collision to the north (Clement et al., 2000; McKenzie, 1978). These major active boundaries are connected through a transform fault zone called the Kefalonia Transform Fault Zone (KTFZ) which is characterized by dextral strike-slip focal mechanisms, with an appreciable thrust component (Kiratzi & Langston, 1991; Papadimitriou, 1988; Scordilis et al., 1985) (Fig. 1a).

The KTFZ consists of two major fault branches, namely the Lefkas branch containing its northern part, striking NNE-SSW and the Kefalonia branch to the south with a slightly different NE-SW strike (Louvari et al., 1999; Papazachos et al., 1998) (Fig. 1b). The southern segment is longer (length ~ 95 km, mean strike 35°), associated with stronger earthquakes in the area and with a maximum reported magnitude of $M = 7.4$ (Papazachos & Papazachou, 2003). The northern segment is shorter (length ~ 35 km) and extends along the western

Supplementary Information The online version contains supplementary material available at https://doi.org/10.1007/s00024-021-02825-9.

[1] Geophysics Department, Aristotle University of Thessaloniki, 54124 Thessaloniki, Greece. E-mail: mponatis@geo.auth.gr; vkarak@geo.auth.gr; ritsa@geo.auth.gr

[2] Istituto Nazionale di Geofisica e Vulcanologia, Via di Vigna Murata 605, 00143 Rome, Italy. E-mail: aybige.akinci@ingv.it

[3] Department of Geophysics and Geothermics, National and Kapodistrian University of Athens, Panepistimiopolis, 15784 Zografou, Greece. E-mail: gkaviris@geol.uoa.gr

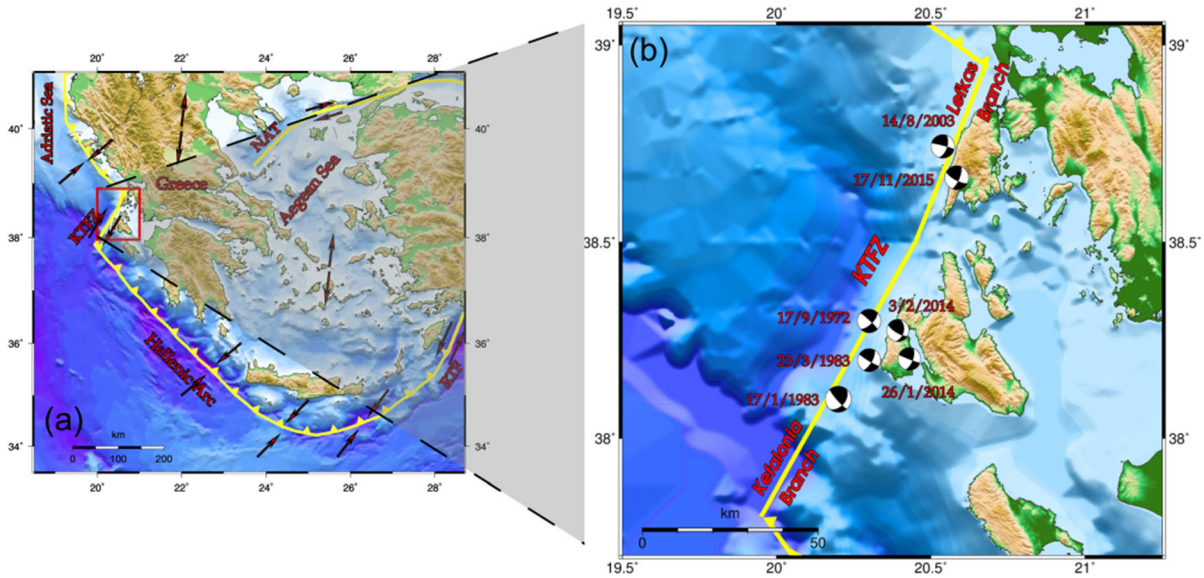

Figure 1

a Main seismotectonic features of the Greek region. The black arrows indicate the approximate direction of the relative plate motion (KTFZ—Kefalonia Transform Fault Zone, NAT—North Aegean Trough, RTF—Rhodes Transform Fault). **b** Major active boundaries in the study area. The subduction front to the south, the KTFZ with the distinctive Kefalonia and Lefkas branches and the collision boundary north of Lefkas Island. The black beach balls indicate the fault plane solutions of the most significant (M ≥ 6.0) recent earthquakes in the region

coastline of Lefkas Island demonstrating a different strike (∼ 15°) in comparison with the southern segment (Karakostas et al., 2004). Strong earthquakes have frequently occurred in this segment as well, with a maximum reported magnitude of M = 6.7 (Papazachos & Papazachou, 2003). The transition zone between these two fault branches has been interpreted as a step-over zone consisting of smaller parallel fault segments striking WSW-ENE (Karakostas et al., 2015). The importance of this explanation lies in the fact that rupture appears to terminate at this location and does not continue further to the north when a mainshock occurs in the southern Kefalonia fault branch and vice versa. Based on this observation, past strong (M > 6.0) earthquakes have been associated with either the Lefkas branch or the Kefalonia branch separately. However, the two fault segments have been activated in the past successively as a result of stress transfer between them (Papadimitriou, 2002).

Despite the high seismic activity, strong ground motion data are limited especially regarding the near-source region, as a consequence of the insularity of the study area. On that premise, realistic ground motion simulations constitute a valuable tool for seismologists to expand the available strong ground motion dataset from past strong earthquakes. The potential of calculating large sets of near-source synthetic seismograms that include realistic source complexity is a powerful tool for up-to-date seismic hazard assessment studies aiming to forecast the strong ground motion and its variability in future strong earthquakes (Graves & Pitarka, 2010; Pitarka et al., 2019; Rogers et al., 2018; Withers et al., 2018).

The first attempts to simulate realistic time series of ground motions were made by Hartzell (1978) and Irikura (1986) who introduced a method of summing the recordings of smaller earthquakes to estimate the expected response of a larger earthquake. Since then, other methodologies have also been proposed to include the source and path effects, as well as other complex characteristics. A thorough review of ground motion prediction techniques was published by Douglas and Aochi (2008).

In the present study, a wave physics-based hybrid approach is adopted to generate broadband strong ground motion seismograms for both the 26th January 2014 Kefalonia M_w6.1 and the 17th November Lefkas M_w6.5 mainshocks. The low-frequency

(hereafter, LF) portion of the synthetic time series was calculated using a 1D wave propagation method, whereas a stochastic finite-fault simulation model was implemented to acquire the high-frequency (hereafter, HF) portion. Finally, the results from the above-mentioned techniques were merged by performing a weighted summation at intermediate frequencies to calculate the broadband synthetic time series.

2. Methodology

Broadband synthetic time histories for the 2014 Kefalonia and 2015 Lefkas mainshocks were generated, by combining a deterministic approach at lower frequencies, with a stochastic approach at higher frequencies. This technique is used worldwide (e.g., Graves & Pitarka, 2004, 2010; Pischiutta et al., 2020) but to a lesser extent for earthquakes in Greece (Ding et al., 2019; Kiratzi et al., 2019; Roumelioti et al., 2016).

2.1. Low-Frequency Ground-Motion Simulations

The LF portion was computed using the discrete-wavenumber finite-element (DWFE) technique of Olson et al. (1984), extended to finite fault discretization (Spudich & Archuleta, 1987; Spudich & Xu, 2002) as implemented in the COMPSYN code (Spudich & Xu, 2002). The representation theorem integral is evaluated on the fault plane and Green's functions are calculated through the DWFE method (Olson et al., 1984) to account for the unit response of the laterally homogeneous velocity model. In this method, after defining the observation locations, Green's functions are computed as tractions on the fault plane, by placing impulsive point load at the receivers' locations, which are then reverted using the reciprocity relation. This allows for the efficient calculation of Green's functions when the number of observation points is small compared to the number of the fault source points (Spudich & Archuleta, 1987). After defining the observation locations, Green's functions are computed as tractions on the fault plane using a reciprocity relation. A kinematic fault model is set as a means to execute the convolution between the Green's functions and the assumed slip and the result is integrated over the surface to generate the ground motion at the selected sites. Eventually, the corresponding synthetic time series are computed through the inverse Fourier transform of the synthetic Fourier Amplitude Spectra (FAS). This simulation technique that computes the seismic wavefield radiated from a source inside an elastic medium is sufficient to produce ground motions up to a transition frequency where source radiation and wave propagation tend to become more stochastic.

2.2. High-Frequency Ground-Motion Simulation

The HF radiation was calculated using a stochastic finite-fault model based on a dynamic corner frequency approach, using the EXSIM code (Assatourians & Atkinson, 2012; Boore, 2009; Motazedian & Atkinson, 2005). The application of EXSIM is based on the definition of a finite fault that is divided into sub-faults, each of which is treated as a stochastic ω^2 point source. Synthetic time series from each sub-fault are simulated using the point-source stochastic method of Boore (1983, 2003). The summation of all contributing sub-faults with the suitable time delay that indicates the rupture propagation across the fault and the combination of source, path, and site effects, results in the calculated ground motions at the sites of interest. The hybrid broadband time series are obtained by merging the LF and HF simulations in the frequency domain, as proposed by Mai and Beroza (2003). This merging technique has the advantage of minimizing the amplitude and phase mismatch between the LF and HF signals by applying frequency-dependent weighted functions and by using an optimization process operating in a narrow frequency range (0.1–0.2 Hz) around a target matching frequency (Mai & Beroza, 2003).

3. Modeling of Past Earthquakes

Strong ground motion simulation requires well-defined source, path and site effects in the area of interest to generate reliable results. Because of the trade-offs between these three main components of

ground-motion, it is necessary to initiate the simulation with high-resolution model parameters. The source and attenuation parameters used in this study are selected from recently published models, released after the M_w6.1 January 26th 2014 Kefalonia, and the M_w6.5 17th November 2015 Lefkas earthquakes (e.g., Chousianitis et al., 2016; Karakostas et al., 2015). The input of the ground motion model is based on the geometry of the finite fault, the rupture velocity, the stress drop, and the seismic moment. An important source parameter is the distribution of slip values along the fault plane. In the following section, we present the detailed description of the two considered earthquakes and the adopted source-related parameters for the ground motion simulations. Although the near-field results are controlled by source effects, such as the slip asperity distribution on the fault plane, the intermediate distance is controlled by path effects, seismic wave propagation, and attenuation. For that reason, the path-related parameters such as the geometric spreading coefficient, the anelastic attenuation the quality factor, the site amplification due to local soil response and the kappa parameter to account for spectral decay at high frequencies are described below.

3.1. The 2014 January 26th Kefalonia M_w6.1 Mainshock

On 26 January 2014 a M_w6.1 mainshock struck the western part of Kefalonia Island, causing considerable damage to infrastructures and triggering a variety of geological and geotechnical effects. The aftershock activity lasted for several months, with the strongest aftershock (M_w5.5) occurring in the first few hours after the mainshock occurrence. On February 3rd, a second mainshock (M_w6.0) occurred on the adjacent fault segment, resulting into the deterioration of damage and additional environmental effects. The slip models determined for the second mainshock were not adequately robust and most near-field data are affected by liquefaction. The GCMT solutions for both mainshocks imply dextral strike-slip motion, with strike = 20°, dip = 65° and rake = 177° for the first mainshock and strike = 12°, dip = 45° and rake = 154° for the second one. According to Karakostas et al. (2015), who performed a high-accuracy relocation of the aftershock sequence, the epicenter of the first event was located at 38.203°N, 20.4308°E with a focal depth of 16 km. The relocated epicenter of the second event was at 38.267°N, 20.323°E with a focal depth of 7 km (Fig. 2a). Relocation with a slightly modified velocity model was also performed by Karastathis et al., (2015) who concluded at a focal depth of ∼ 16 km for the 26/01/2014 mainshock and a seismogenic layer confined between 6 and 15 km. A fault starting at 7 km and a down-dip edge at 27 km, with a fixed focal depth for the mainshock at 16 km, was considered by Papadopoulos et al. (2014) who suggested a slip model with a downward rupture evolution. The slip model of Sokos et al. (2015) revealed an up-dip propagation, reaching shallow depths and then continuing to propagate predominantly towards the north. Both models concluded to the same main slip patch, but they considerably differ due to the diversity of the assumed fault planes and the data used. An up dip-slip evolution was suggested by Millas (2018) as well, with the slip mainly concentrated in one main patch that was developed shortly after the rupture nucleation.

3.2. The 17th November 2015 Lefkas M_w6.5 Mainshock

On 17 November 2015 (07:10:07 GMT) a M_w6.5 mainshock occurred on a fault segment which is extended along the southwestern coastline of Lefkas Island. The earthquake was felt in an extended area covering the Ionian Islands, western Greece, Peloponnesus, and the south coast of Italy. This is one of the strongest reported earthquakes in Lefkas Island, especially in the instrumental era, compared only to the first mainshock of the 1948 doublet, which also ruptured the SW part of the Island (Papazachos & Papazachou, 2003). All available determined focal mechanisms suggest a right-lateral strike-slip fault striking NNE-SSW, parallel to the western coastline, in agreement with the orientation of the KTFZ at this location (Ganas et al., 2016; Papadimitriou et al., 2015, 2017; Sokos et al., 2016). The GCMT solution for the mainshock reveals a plane striking at 16°, dipping 64° to the ESE, with a rake of 179° (Fig. 2a). The documented slip distribution models indicate that

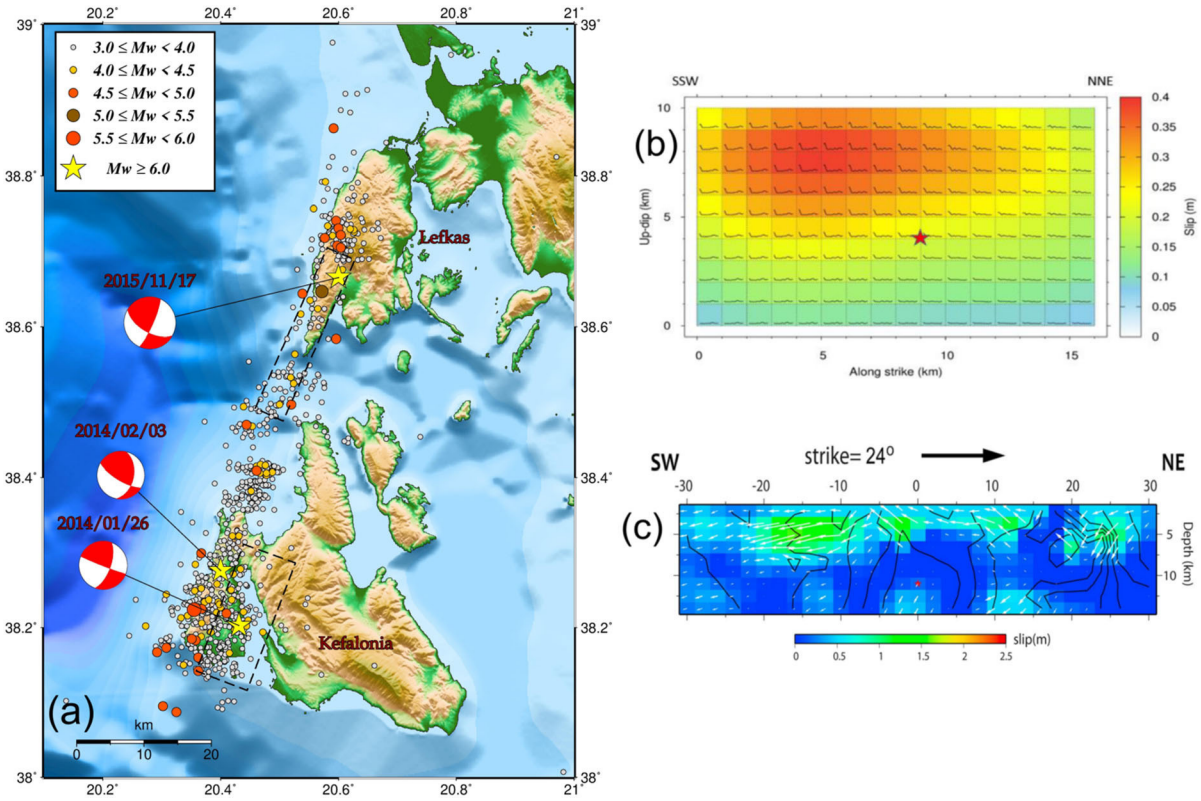

Figure 2
a Locations of the two selected earthquakes along with the epicentral distribution of the earthquake sequences (adopted by Karakostas et al., 2015). The focal mechanism for the Kefalonia M_w 6.1 2014 event corresponds to the GCMT solution and **b** the slip distribution model was adopted by Millas et al., (2018). The focal mechanism for the Lefkas M_w6.5 2015 event was obtained by Zahradnik and Sokos (2016), whereas **c** the slip distribution model was adopted from Chousianitis et al., (2016)

most of the slip is up-dip from the hypocenter at depths shallower than 10 km. In addition to the larger slip asperity located close to the nucleation point, a smaller one, located to the NE of the mainshock epicenter has been inferred, suggesting bilateral rupture propagation (Avallone et al., 2017; Chousianitis et al., 2016). A relatively complex slip pattern with a heterogeneous distribution was found by Chousianitis et al. (2016). They proposed that the slip was confined in the upper 10 km, where two main asperities, one with peak slip amplitude of 2.35 m to the southwest of the epicenter, releasing the 65% of the total seismic moment, and a smaller one to the northeast of the epicenter were observed. However, they have provided several solutions determined using various datasets (e.g., teleseismic, strong ground motion and high-rate GPS data) for the finite fault model. Bilateral propagation with three slip patches is implied according to the slip model proposed by Avallone et al. (2017).

3.3. Stochastic Modeling Parameters

The spectrum of the ground motion is affected and includes the source, path and site components (Boore, 1983, 2003). Certain parameters of each component must be defined to perform the HF ground motion simulations. The full set of parameters employed in the stochastic finite-fault modeling for the 2014 Kefalonia M_w6.1 and 2015 Lefkas M_w6.5 mainshocks are summarized in Table 1. In this section, the main model input parameters and selected values are justified and described.

Table 1

Modeling parameters used for the High Frequency finite-fault stochastic method application performed with the EXSIM code

Parameter	*Kefalonia 2014* Value	*Lefkas 2015*
Source		
Moment magnitude	6.1	6.5
Fault area	20 × 20 km^2	28 × 15 km^2
Fault geometry	Strike = 20°, Dip = 65°	Strike = 24°, Dip = 80°
Depth of the fault plane top	9.00 km	0.66 km
Sub-fault size	1.0 × 1.0 km^2	2.0 × 1.5 km^2
Slip model	Millas et al. (2018)	Chousianitis et al. (2016)
Stress parameter	130 bars	65 bars
Sub-fault window	Exponential	
Rupture velocity	0.8V$_s$	
Rise time	$1/f_0$ (Inverse of sub-fault corner frequency)	
Pulsing %	50%	
Path		
Geometrical spreading	$R^{-1.0}$ for R < 100 km	
Anelastic attenuation	Q = 275(f/0.1)$^{-2}$ f ≤ 0.2 Hz Q = 88 (f/1.0)$^{0.9}$ f ≥ 0.6 Hz	
Crustal shear-wave velocity	3.4 km/s	
Crustal density	2.7 g/cm^3	
Site		
Site and crustal amplification	Table 2	
Kappa	0.035	

3.3.1 Source Parameters

The source parameters include the fault orientation (strike and dip) and dimensions, the fault burial depth, the position of the hypocenter on the fault plane, the moment magnitude, the slip distribution onto the fault surface and the stress parameter ($\Delta\sigma$). Regarding the 2014 mainshock, plenty of trials with different models were performed due to the large discrepancy between the proposed fault and slip distribution models (e.g., Papadopoulos et al., 2014; Sokos et al., 2015). The fault and focal parameters were obtained from the high-accuracy relocation of Karakostas et al. (2015) and the slip distribution model was adopted from Millas et al. (2018) (Fig. 2b). The proposed slip distribution models of the Lefkas 2015 mainshock (e.g., Avallone et al., 2017; Chousianitis et al., 2016; Sokos et al., 2016) indicate relatively similar fault setting and slip distribution. The selection of the appropriate slip model for the latter case was achieved through the comparison of the synthetic with the recorded acceleration spectra. On that premise, one of the slip distribution models of Chousianitis et al. (2016) that was determined using the strong motion and 1 Hz GPS data, was used for the simulations (Fig. 2c), along with the focal parameters obtained from the moment tensor solution of Zahradnik and Sokos (2015). To demonstrate the sensitivity of our simulations at near-source distances to the source rupture slip model, we have also adopted a source slip model proposed as "preferred" model by Chousianitis et al. (2016), obtained through the joint inversion of geodetic, teleseismic and strong motion data. The alternative slip model and the related simulations are presented in Online Appendix A (Figures S1–S3).

The stress parameter ($\Delta\sigma$) is a crucial parameter and the most difficult to determine in the context of stochastic ground motion modeling. The initial stress parameter value used in the simulations is the mean value derived from Margaris and Boore (1998) and Margaris and Hatzidimitriou (2002) for strong (M > 5.8) earthquakes in Greece. Their mean value of $\Delta\sigma$ = 56 bars is close to the average value (60 bars) computed by Kanamori and Anderson (1975) for an integrated data sample of both intraplate and interpolate earthquakes. In this study, various stress drop values around the adopted one were tested, comparing the resulting simulated ground motions in terms of PGA and PGV with the observed ones using a trial-and-error approach. For the 2014 Kefalonia mainshock that was nucleated at a larger focal depth, the visual comparison of simulated and observed FAS and the direct comparison of simulated and observed PGA values from the available recordings indicated that such high values could not be reached.

Since the available strong-motion data are scarce in the region, we used the empirical ground motion predictions to calibrate the stress drop parameters for both earthquakes. A trial-and-error approach has been applied by calculating the misfit between the simulated and the three GMPE-derived ground motions

(see for details Sect. 4.2) for both the 2014 Kefalonia and the 2015 Lefkas earthquakes. The comparison of misfits was based on the combination of horizontal PGA and PGV values in terms of their geometric mean. As it is observed in Fig. 3a, b, the values of $\Delta\sigma$ = 130 and 65 bars were considered the most suitable and proved to provide a satisfactory match between the simulated and the estimated ground motions from the GMPEs for the M_w6.1 Kefalonia and M_w6.5 Lefkas earthquakes, respectively. Similar high values of $\Delta\sigma$ (180 bars) have also been used in stochastic simulations at Kefalonia Island by Mouzakiotis (2015) who performed stochastic ground motion simulations in selected sites in Greece whereas the $\Delta\sigma$ = 65 bars value determined for the 2015 Lefkas mainshock is also similar to the one suggested by Margaris and Boore (1998) and Margaris and Hatzidimitriou (2002).

3.3.2 Path Parameters

Geometrical spreading, attenuation and path properties are also critical parameters that must be set to account for the path effects. The geometric spreading function was set equal to 1/R for distances up to 100 km (Margaris & Boore, 1998). For the anelastic attenuation, which is controlled by the quality factor (Q), the model of Boore (1983) which is in good agreement with later studies investigating the Q value in Greece (Hatzidimitriou, 1995; Hatzidimitriou et al., 1993), was used (Eq. 1).

$$\begin{aligned} Q &= 275(f/0.1)^{-2.0}, \quad f \le 0.2\text{Hz} \\ Q &= 88(f/0.1)^{0.9}, \quad f > 0.6\text{Hz} \end{aligned} \tag{1}$$

Q values for frequencies between 0.2 and 0.6 Hz are determined from power-law fit to values of Q at f = 0.2 and f = 0.6 Hz.

3.3.3 Site Properties

The parameters employed to quantify the impact of the shallower sedimentary layers to the seismic motion are the kappa parameter and the soil amplification factor. The kappa (κ_0) parameter is defined as an exponential decay to represent the diminution factor (Anderson & Hough, 1984) and can be regarded as a low-pass filter. The diminution factor D(f) used in the stochastic modeling, in relation with the kappa filter is expressed by:

$$D(f) = e^{-\pi\kappa_0 f} \tag{2}$$

Multiple studies have been conducted in order to determine the kappa values applicable for strong earthquakes in Greece. Hatzidimitriou et al. (1993)

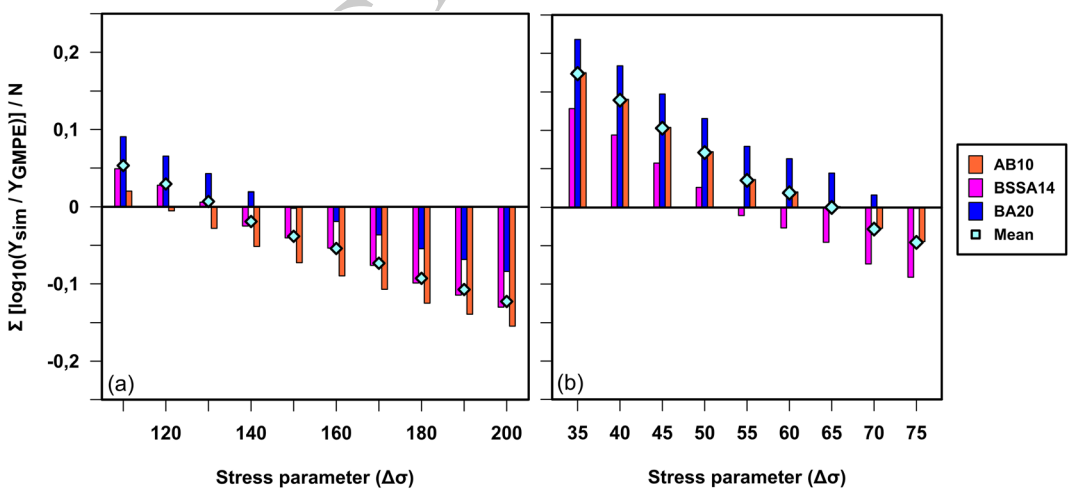

Figure 3
Residuals between simulated and GMPE-derived PGA and PGV values **a** for the Kefalonia M_w6.1 earthquake determined using 10 stress parameter ($\Delta\sigma$) values, ranging from 110 to 200 bars; **b** for the Lefkas M_w6.5 earthquake calculated over 9 stress drop parameters ranging between 35 and 75 bars

used a dataset of strong motion recordings at sites varying from very soft to stiff soil conditions and estimated an average κ_0 value of 0.06. The same average value was also obtained from Margaris and Boore (1998), though for class B sites the corresponding value diminishes to 0.035. In latest studies (Klimis et al., 1999), kappa values for NEHRP (National Earthquake Hazards Reduction Program) class C (0.044) and D (0.066) Greek sites were determined in an effort to provide frequency-dependent amplification factors following a classification system. In the present study, the spectral decay factor kappa (κ_0) was set as 0.035, which corresponds to class B (Vs_{30} between 760 m/s and 1500 m/s) of the NEHRP classification and the appropriate frequency-dependent site attenuation factors for this soil type (Table 2) were adopted from Margaris and Boore (1998).

3.4. Deterministic Modeling Parameters

The LF portion of the synthetic ground motions is calculated using kinematic source modeling and the discrete wavenumber finite element (DWFE) method by applying the COMPSYN code (Spudich & Xu, 2002). The numerical techniques of Spudich and Archuleta (1987) implemented in the framework of the COMPSYN code require the definition of parameters related to the crustal velocity structure, the fault characteristics and the earthquake slip distribution. The Earth's crust was modeled as a vertically layered medium to account for the changes in density and wave propagation velocity as a function of depth. For this purpose, the velocity model for the Ionian Islands suggested by Papadimitriou et al. (2017) was adopted (Table 3). The density for all layers of the velocity model was computed using the relationship of Gardner et al. (1974):

$$\rho = 0.31 V_p^{0.25} \quad (3)$$

where ρ is the density in kg/m^3 and V_p is the P-wave velocity measured in m/s.

As far as the kinematic parameters are concerned, the same slip distribution models employed in the HF portion simulations were used (Fig. 2b,c). A boxcar source time function was adopted and considered the same at all points of the fault. The rise time was considered constant at all grid points, equal to 1 s, therefore, the rise time variability across the fault plane was not taken into account in this study. The rupture front was assumed to be circular propagating outward from the nucleation point, having a rupture velocity equal to 3 km/s for the 2014 Kefalonia mainshock, as indicated by Papadopoulos et al. (2014) and 2.5 km/s for the 2015 Lefkas mainshock according to Chousianitis et al. (2016). Following this assumption, the rupture time at each node considered on the fault surface was determined based upon the time when the rupture front reaches its position.

Table 3

Velocity model proposed by Papadimitriou et al. (2017). Density values in the 4th column were computed according to the Gardner et al. (1974) relationship

Upper depth of layer (km)	P-wave velocity (km/s)	S-wave velocity (km/s)	Density (g/cm^3)
0	5850	3145	271
1	5870	3156	271
2	5980	3215	272
6	6235	3352	275
8	6490	3489	278
9	6525	3508	278
11	6560	3527	278
13	6580	3538	279
21	6625	3562	279
28	6700	3602	280
40	8000	4301	293

4. Hybrid Ground Motion Simulation Results

The hybrid broadband simulation results are discussed in this section. The LF component derived from the deterministic simulation and the stochastic HF component were merged in the frequency domain as proposed by Mai and Beroza (2003). The transition frequency range of 0.8 and 1.5 Hz between the two portions of the synthetics was selected to ensure that the broadband synthetics contain all the LF near-field terms and approximate satisfyingly the HF contributions. Figure 4 illustrates an example of the implementation of a hybrid broadband horizontal seismogram obtained after filtering and summation of the deterministic LF and random HF composition.

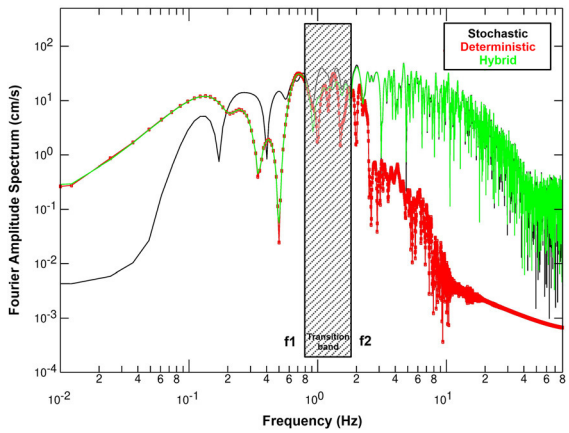

Figure 4
Example of the calculation of hybrid broadband seismograms (ITC1 station). Broadband seismogram (green) calculated by combining the LF seismogram (red) with the region-specific HF seismogram (black) in a Fourier domain

4.1. *Spatial Distribution of Simulated Strong Ground Motion*

In an effort to better assess the ground motion variability caused by the two strong earthquakes, a normal grid superimposed on the study area was used, with its nodes at a spacing of 0.05°, which corresponds to 1271 and 1681 virtual stations for Kefalonia 2014 and Lefkas 2015 mainshocks, respectively. Synthetic records of acceleration and velocity for each node were simulated, assuming uniform soil B type for the local site conditions. Figure 5a, b show the spatial distribution of simulated PGA and PGV values for the M_w6.1 26th January 2014 mainshock, which mainly reflects the source effect, given that the soil condition is assumed to be uniform. The PGA distribution in Fig. 5a shows that the strongest ground shaking took place in the vicinity of the area around the main asperity of the activated fault (Fig. 2b). This illustrates that slip heterogeneity within the source dominates in the near-field strong ground motions rather than the average slip in the entire rupture area (Irikura & Miyake, 2011). The simulated PGA and PGV spatial distributions are in agreement with the spatial distribution of damage and other earthquake-induced geological effects, as well as macroseismic intensity maps (e.g., Papadopoulos et al., 2014; Valkaniotis et al., 2014). The PGA and PGV distributions in Fig. 5a, b show that the strongest ground motion occurs near the large slip release. The largest slip patch is located at the center of the fault plane, slightly to the south. The ground motions obtained through the stochastic simulation provided the maximum values of PGA and PGV of 0.4 g and 25 m/s, respectively. The computed PGA value at Lixouri (405 cm/s^2) is, however, slightly underestimated compared to the recorded one (Table 4). This deviation can be explained by the fact that the station (LXRB) is on the surface projection of the activated fault, therefore it is considerably more affected by the source complexity and other near-source effects. The position of the slip asperity and the slip amplitude might be mislocated in the source model adopted for our simulations. This presumably explains the presence of PGA values closer to the recorded one in neighboring nodes of the grid offshore LXRB station. The observed PGA and PGV values are much more scattered over the rupture fault plane at near source distances, ($R_{jb} < 10$ km) presenting strong variations in ground motion amplitudes (ranging between 200 and 400 cm/s^2) characterized by local minima and maxima with respect to those at intermediate and longer distances where the influence of the slip distribution becomes negligible (Fig. 5a).

The simulated PGA and PGV values for the M_w6.5 17th November 2015 mainshock obtained using EXSIM, are presented in Fig. 6a, b, where it is highlighted that the main slip asperities have a major influence on the regions suffering the strongest ground shaking. The simulated PGA values match quite well the recorded data (Table 4), however, a slight overestimation is observed on the closest recording (VAS2, $R_{jb} \sim 1.5$ km), with the simulated value being 412 cm/s^2 and the recorded 363 cm/s^2. This slight deviation again could possibly be explained by the fault slip model that was used in the simulations, given that the position of the slip asperities has a great impact on ground motions for site-to-site comparisons. However, in general, the comparison with the damage (and other earthquake-induced phenomena) distribution maps reveals a reasonable agreement with the spatial distribution of the simulated PGA and PGV values. After the evaluation of macroseismic intensity maps (Papathanassiou et al., 2017) it is observed that the isoseismal pattern coincides with the ones shown in

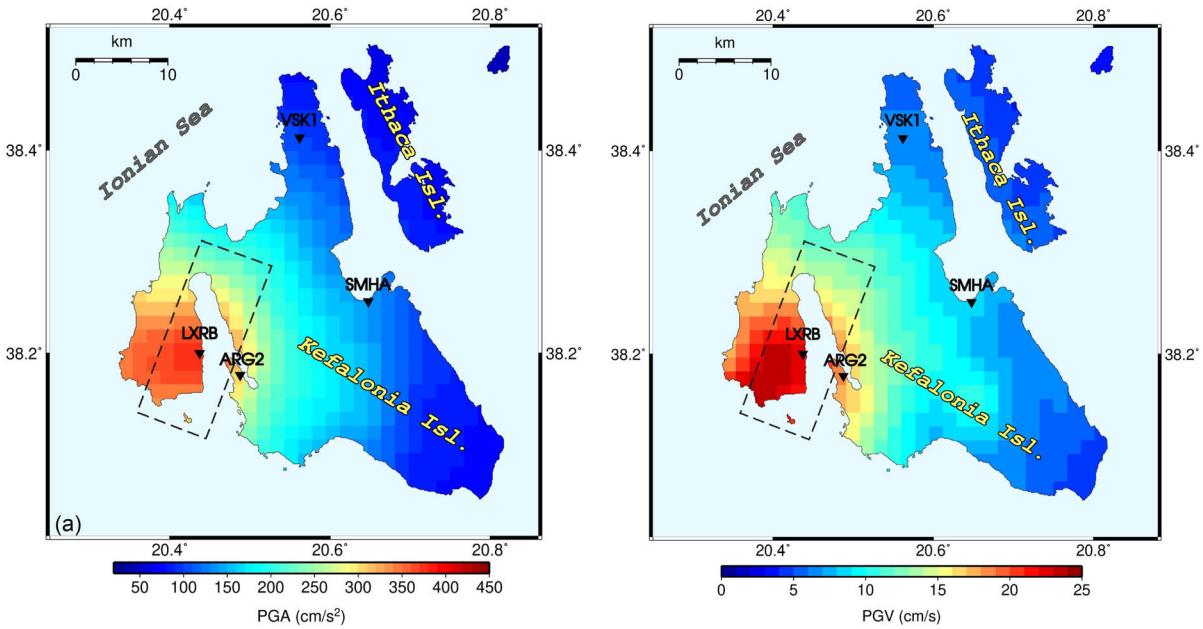

Figure 5
Spatial distribution of simulated **a** PGA (cm/s^2) and **b** PGV (cm/s) values calculated with the EXSIM code for the 26th January 2014 Kefalonia mainshock, using the parameters given in Table 1

Table 4

Selected accelerometric stations providing the strong motion data for the (a) 26th January 2014 Kefalonia and the (b) 17th November 2015 Lefkas mainshocks. In the last column, the PGA values resulted from the hybrid broadband simulations are presented

	Station	Code	Owner	Epicentral distance (km)	Soil class	Recorded PGA (cm/s^2)		Simulated PGA (cm/s^2)	Recorded PGV (cm/s)		Simulated PGV (cm/s)
						N-S	E-W		N-S	E-W	
(a)	Argostoli	ARG2	ITSAK	13	B	348	393	344	20	14	18
	Vasilikiades	VSK1		34	A	95	78	88	8	5	5
	Lixouri	LXRB	NOA—IG	10	B	561	425	405	30	61	19
	Sami	SMHA		29	–	269	238	143	16	15	9
(b)	Vassiliki	VAS2	ITSAK	8	B	363	226	412	29	17	29
	Lefkas Town	LEF2		21	B	102	86	76	8	7	9
	Ithaca	ITC1		35	–	117	79	120	5	6	9

Fig. 6a, b especially in the region where the highest simulated PGA values were obtained (SW Lefkas).

4.2. *Comparison with GMPEs*

In order to compare the simulated ground motions obtained using EXSIM, the three GMPEs of Boore et al. (2020) (hereafter, BA20), Boore et al. (2014) (hereafter, BSSA14) and Akkar and Bommer (2010) (hereafter, AB10) were used. The former is the most recently proposed GMPE derived using a uniformly processed strong motion dataset compiled using the Greek accelerometric archives. The second one was developed within the context of the Next Generation Attenuation (NGA) models from the worldwide strong-motion recordings, whereas the latter is derived as the Europe and Middle east GMPE model by Akkar and Bommer (2010) using a strong-motion

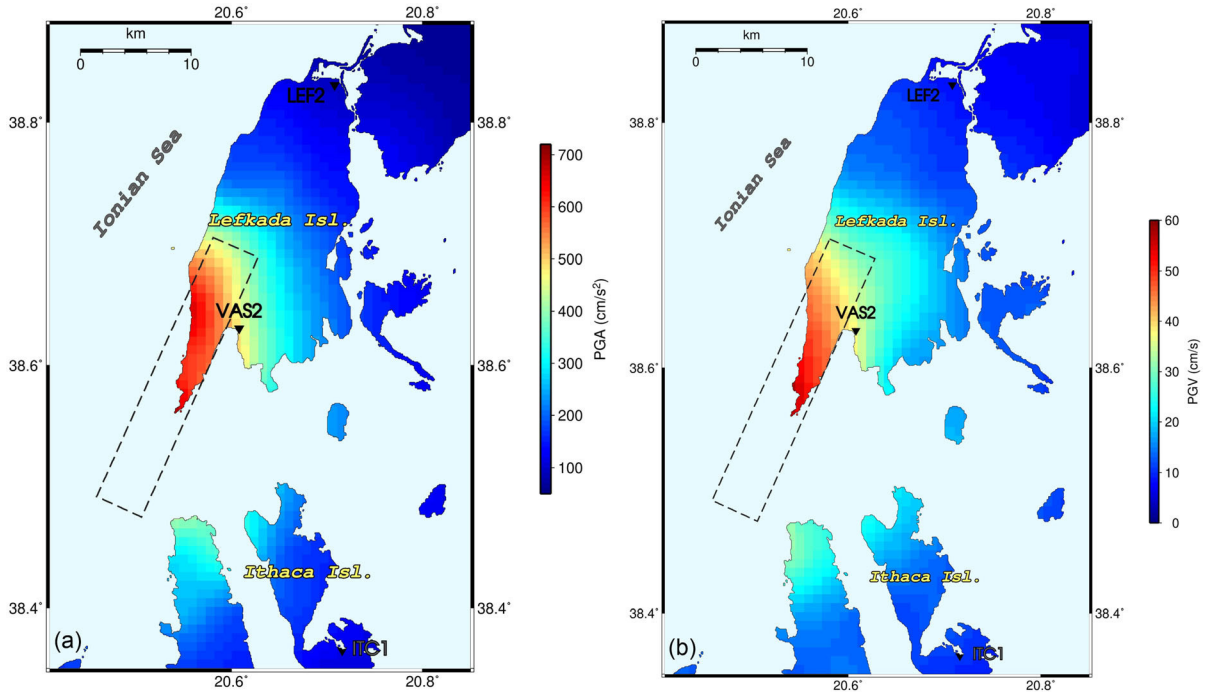

Figure 6
Spatial distribution of simulated **a** PGA (cm/s^2) and **b** PGV (cm/s) values calculated with the EXSIM code for the 17th November 2015 Lefkas earthquake, using the parameters given in Table 1

dataset mostly from Turkey, Italy and Greece and is suggested to be used for crustal earthquakes in active shallow crustal regions.

Figure 7a, c show the comparisons for PGA and PGV, respectively, regarding the M_w6.1 2014 Kefalonia mainshock. 57 horizontal PGA values recorded from the stations of the Hellenic Unified Seismological Network (HUSN) are plotted, at distances up to 198 km as a function of the Joyner & Boore distances (hereafter, R_{jb}) and compared with the values derived from the selected GMPEs, as well as with the simulated PGA values for 1271 dummy stations using the EXSIM code. The simulated values that lie on the surface projection of the fault ($R_{jb} = 0$) are assigned with a very small positive R_{jb} value so that they are visible in the logarithmic scale. The GMPEs are obtained for strike-slip faulting style and type B soil condition. As it can be seen from Fig. 7a, the simulated PGA values generally show good agreement for the entire distance range with the recordings and the GMPE curves. Moreover, the simulated PGA values match quite well with the trend of the observed PGAs at larger distances ($R_{jb} > 70$ km), decreasing faster than the predicted by AB10, indicating a strong seismic wave attenuation by distance. The BA20 and BSSA14 models that were obtained using the Greek and NGA strong motion databases, respectively, capture this feature adequately. The adopted GMPEs present different levels of PGA and PGV amplitudes in the distance ranges 0–20 km and well separated from each other. This can be attributed partly to the lack of sufficient near-fault strong motion data, particularly from intermediate and large earthquakes ($M > 6.5$), which has an impact in the development of the GMPEs and their applicability in the near-field. Thus, it is difficult to fully assess the ground motion variability in smaller R_{jb} distances, caused by the source and the fault rupture complexity due to its natural stochastic behavior.

To better assess the fit between the PGA and PGV values obtained from the stochastic simulations (Y_{syn}) and the ones derived from the GMPEs (Y_{GMPE}), residuals were calculated by the equation:

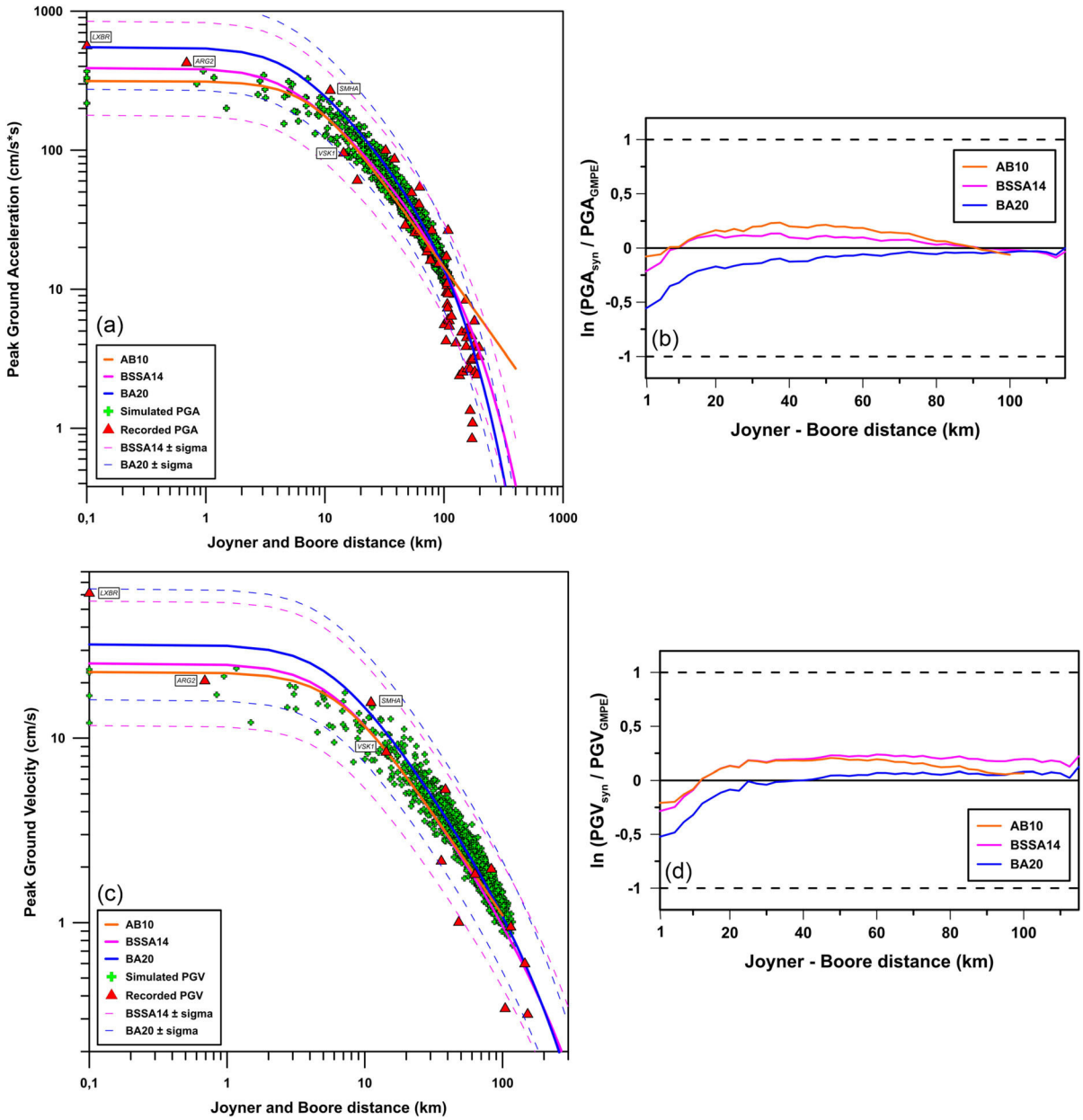

Figure 7
Comparison between the recorded (triangles), GMPE-derived (lines) and simulated (crosses) **a** PGA and **c** PGV values for the January 26th 2014 M_w6.1 Kefalonia earthquake. Residuals between the simulated **b** PGA and **d** PGV values and the values obtained from the use of AB10, BSSA14 and BA20 GMPEs, plotted as a function of the Joyner & Boore distance, R_{jb}

$$R = \ln(Y_{syn}) - \ln(Y_{GMPE}) = \ln(Y_{syn}/Y_{GMPE}) \quad (4)$$

The ground motion variability is illustrated in Fig. 7b, d as a function of the R_{jb} distance from the fault. Figure 7b evinces that the overall PGA variability is placed inside the ± 1 sigma range of the GMPEs. Regarding PGA, the residuals from the two GMPEs, BSSA14 (pink line) and AB10 (orange line) are inside the ± 0.25 standard deviation (σ) interval. The BA20 residuals (blue line) are also in

the same range, apart from a spike in the near-field (0–10 km) where they reach up to − 0.5σ. Although the simulations overestimate the AB10 and the BSSA14 ground motion predictions, they are underestimated by the BA20 model in terms of PGA up to the intermediate distances ($R_{jb} < 60$ km). The fit between simulations and GMPEs gets better at larger distances, $R_{jb} > 60$ km (Fig. 7b). A similar impression is provided by the equivalent PGV graph (Fig. 7c), where the values derived from the GMPEs correlate well with the simulated values. As shown in the same figure, both the simulated and the recorded PGVs are more dispersed than the PGAs, which poses a challenge to find empirical models with better consistency in closer distances. Most PGV residuals fall within the range ± 0.25σ of the three empirical equations at distances $R_{jb} > 20$ km (Fig. 7d). The simulated PGVs are slightly underestimated at the short distance ranges (0–20 km) and overestimated at the longer distances ($R_{jb} > 20$ km) by the GMPEs. The differences between the simulated and empirically estimated values derived from the GMPEs cannot be assessed successfully for very near-source distances given that the GMPEs were established using a very limited near-source dataset where the largest ground motion variability is observed.

The same validation procedure was conducted for the M_w6.5 2015 Lefkas mainshock. As Fig. 8a shows, the simulated PGA values appear to have a matching trend with the 17 horizontal PGA values recorded from the HUSN stations, as well as with the ones derived from the GMPEs, particularly in distances over 10 km. Additionally, in the entire R_{jb} range, the simulated PGA values lie within the ± 1 standard deviation area. All residuals from the three GMPEs, BSSA14 (pink line), BA20 (blue line) and AB10 (orange line) are almost inside the ± 0.25 standard deviation interval. As it can be seen in Fig. 8b the empirical predictions of BSSA14 and AB10 present lower peak ground acceleration values in shorter distances ($R_{jb} < 50$ km) and gradually larger at the longer distances ($R_{jb} > 50$ km) compared to those estimated by the simulations. The BA20 ground motion model presents larger peak ground accelerations over all the distance motions against the simulations. However, the simulations show good agreement with the observed data over all the distance ranges (0–100 km). In the same context, it is evident that the ground motion parameters are less scattered and more stable at longer distances away from the inferred fault trace, because of the gradually decreasing influence of the slip distribution in the far field. Figure 8c shows the simulated PGV values for the same virtual stations previously used with the application of the EXSIM code, compared to the values derived from the selected GMPEs in their appropriate formulation to account for ground velocity. The simulated PGV values are placed inside the ± 1 sigma range of the GMPEs. However, the closest recorded value, corresponding to the smaller R_{jb} distance is slightly underestimated both by the empirical GMPE models and the simulations. Nevertheless, the general trend is well represented in the entire distance range. In contrast to Fig. 8b, the PGV variability (Fig. 8d) reveals a better fit in the near-source area and it slightly grows as the R_{jb} increases, displaying several fluctuations, yet it never exceeds 0.5σ. Aiming to highlight the sensitivity of ground motion amplification pattern to the fault rupture and the slip distribution, we adopted one of the slip models calculated through the joint inversion of several datasets by Chousianitis et al. (2016) (Online Appendix A). This model exhibits different high slip patches compared to those shown in Fig. 2c.

4.3. Comparison with Observed Strong Motion Data

The Fourier amplitude spectra of the simulated ground motions at the selected stations are compared with the available strong motion records and presented in Figs. 9,11. The simulated acceleration and velocity time series are also compared with the observations (Figs. 10, 12). The comparison of the hybrid synthetics with the recorded data of the 2014 Kefalonia mainshock reveals a satisfactory fit both in amplitudes and envelope shapes. The simulated PGA and PGV values are close to the level of the recorded ones (Table 4). Broadband velocity time series (Figs. 10b, 12b) also show a satisfactory fit with the recorded data. However, the recorded seismic signal at LXRB station exhibits a low frequency content that is not well reproduced by the simulations. The presence of low frequency velocity pulses in near-fault ground motions is not uncommon since they are

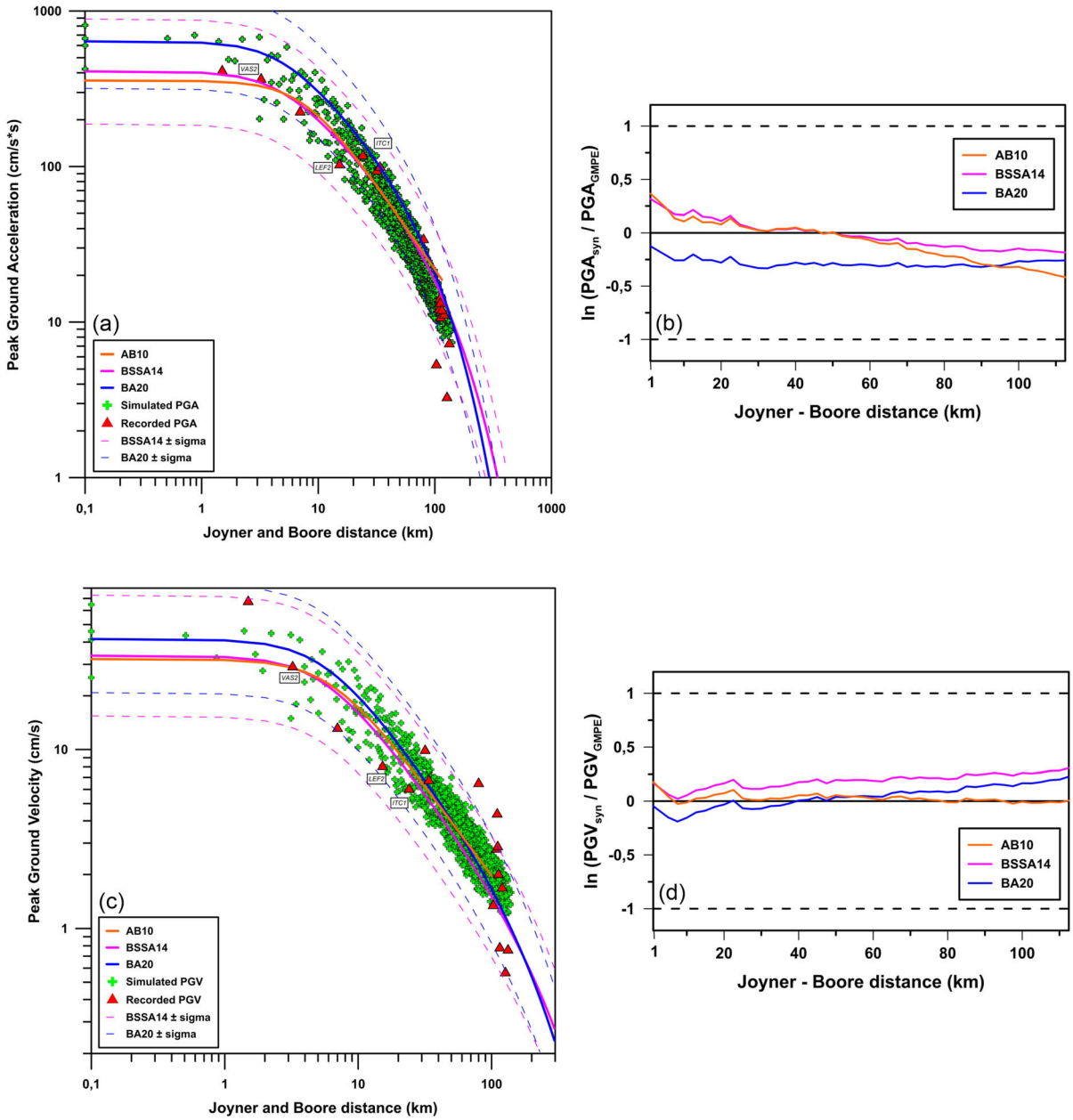

Figure 8
Comparison between the GMPE-derived (**lines**) and simulated (crosses) **a** PGA and **c** PGV values for the November 17th M_w6.5 Lefkas earthquake. Residuals between the simulated **b** PGA and **d** PGV values and the values obtained from the use of AB10, BSSA14 and BA20 GMPEs, plotted as a function of the Joyner & Boore distance, R_{jb}

affected by directivity phenomena, usually associated with the direction normal to the fault. It should also be mentioned that in several locations around LXRB station, such as the port of Lixouri, typical liquefaction phenomena were observed after the mainshock occurrence (Theodoulidis et al., 2016) which may introduce further complexities to the recorded signal. Moreover, the large variations in the earth's crust depth-velocity structure and the appreciable topographic changes require a site-specific velocity model

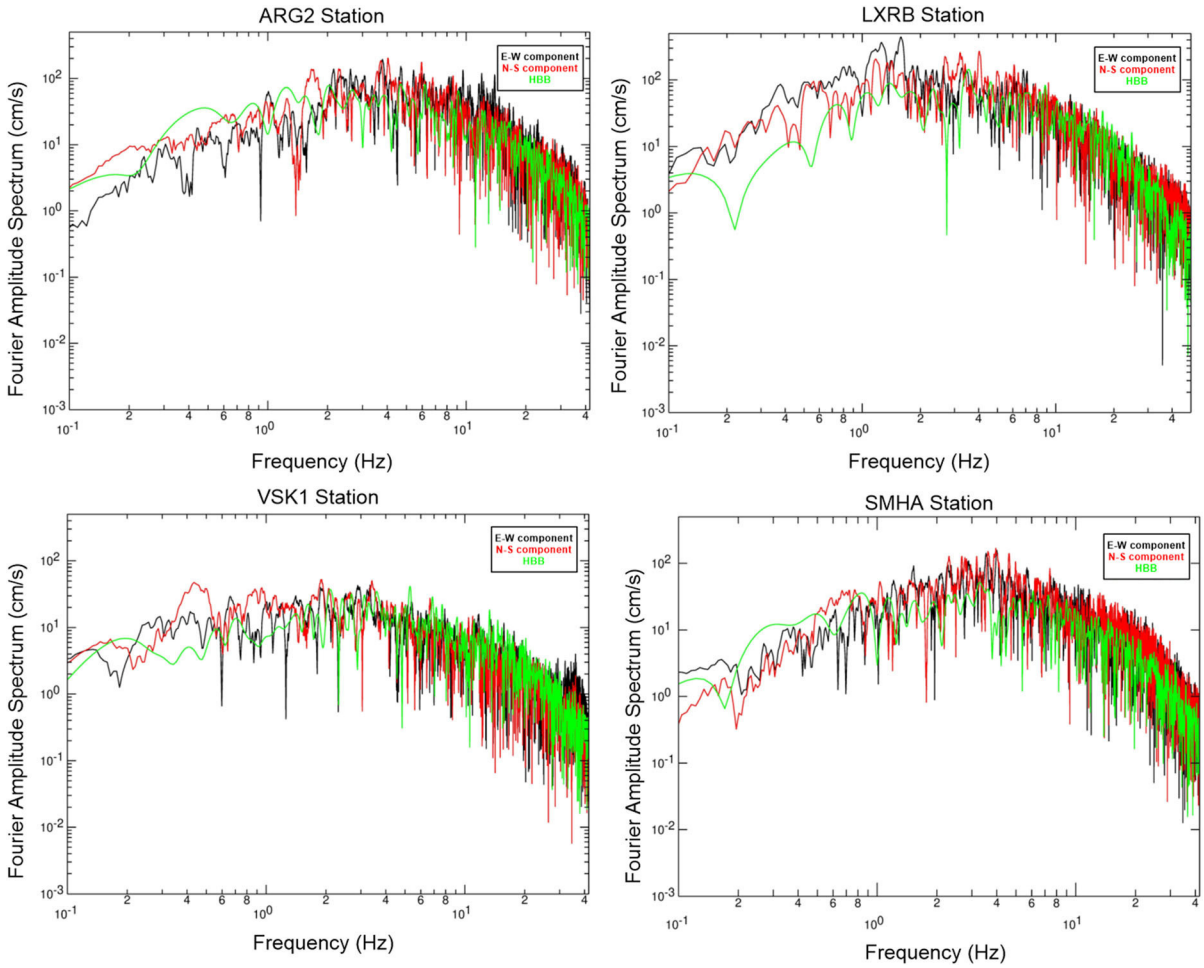

Figure 9
Fourier amplitude spectra for the January 26th 2014 M_w6.1 Kefalonia earthquake at four selected stations (red and black lines correspond to N-S and E-W components respectively) in comparison with the simulated ground motions (green lines) obtained using the hybrid approach

to capture the overall site effect of the study area. In addition, a one-dimensional crustal structure is used for the LF seismograms, which may be simplistic to capture the 2D/3D effects, such as reverberations, converted waves throughout the model and methods considered in this study. In general, the shape of the simulated spectra matches very well the recorded ones in the entire frequency band, which was a key objective of the present study. The duration of the simulated time series, however, seems to be slightly decreased when compared to the recorded time series, especially as the epicentral distance increases. This can be attributed to the reflected waves that reach the more distant stations and add further complexities to the signals. More specifically, the simulated PGA value for ARG2 (0.35 g) station is in close proximity with the recorded one (0.38 g) and the same applies to the more distant stations VSK1 (0.09 g) and SMHA (0.15 g) where the recorded PGA (0.09 g and 0.26 g respectively) values are in direct proximity. On the contrary, the simulated PGA value for LXRB (0.41 g) station is underestimated compared to the recorded one (0.50 g) and the same applies to the corresponding PGV values (Table 4). It is important to note that stations grounded in rock or other rock-like geological formations (e.g., VSK1 station, which is installed on an area consisted mainly of limestones) provide better fit to the simulated data in comparison

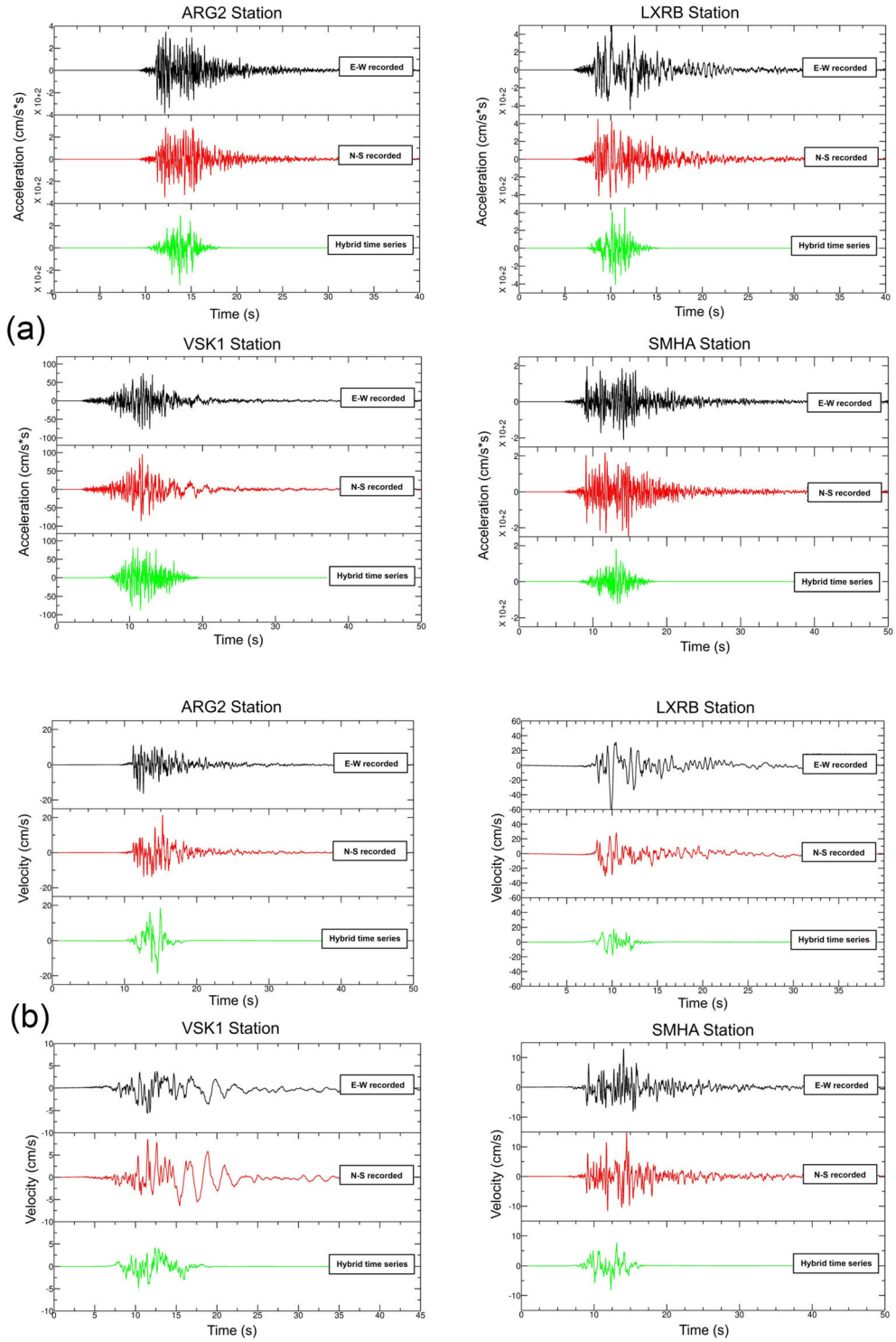

Figure 10
Comparison between recorded (red and black) and synthetic (green) broadband **a** acceleration and **b** velocity time series for the four selected stations for the January 26th 2014 M_w6.1 Kefalonia earthquake

with other stations (e.g., LXRB and ITC1 stations) whose location either approaches soft rock and dense soil condition or is unspecified.

Regarding the 2015 Lefkas mainshock, the comparison between the hybrid synthetics and the recorded data indicates a satisfactory fit both in amplitudes and envelope shapes. The simulated PGA and PGV values are relatively close to the recorded ones (Table 4). In more detail, the PGA values simulated for LEF2 (0.08 g) and ITC1 stations (0.12 g) and the recorded ones (0.10 g and 0.12 g, respectively) are very close. However, at the closest station to the fault surface projection (VAS2) the simulated PGA values (up to 0.42 g) seem to be rather overestimated compared to the recorded ones (up to 0.36 g). Furthermore, the general shape of the simulated spectra fits well to the recorded spectra in the entire frequency band, especially at ITC1 station, although the simulated PGA values and the duration of the time series are higher. As mentioned previously, the observed variation of the ground motion parameters, particularly at near-fault distances, could be attributed to the imperfection of the adopted source model and the related parameters (position of the local slip, the rupture velocity, etc.). It becomes quite challenging to have a perfect fit between recordings and simulations, especially for end-to-end and site-to-site comparisons in a complete frequency range (0–20 Hz), since the considered method (hybrid-broadband approach) does not completely solve the high and low frequency wave field together in a 3D crustal structure containing all direct arrivals, converted phases and surface waves. However, in near-fault areas, we have observed that, compared with using GMPEs, hybrid simulation has a higher ability to detect near-source effects and reproduce source complexity to some extent.

5. *Discussion and Conclusions*

The accurate simulation of strong ground motion remains one of the most critical issues in modern seismic hazard studies and Engineering Seismology (Mai, 2009). Reliable broadband strong ground motion simulations can be extremely useful, especially for regions with limited availability of strong ground motion data, since they can provide peak ground motion parameters and their frequency content for scenario earthquakes, in order to fill in the gaps of the available seismic databases. They are also important as a means to understand the earthquake mechanisms and the characteristics of the propagation path in a certain area. The use of GMPEs could be adequate in some cases, but due to their inefficiency to account for the near-field complexities, the optimum way to simulate ground motions is to compute broadband synthetic time series.

For the scope of this study, a hybrid broadband simulation approach was applied to simulate ground motions for the 26th January 2014 (M_w6.1) and 17th November 2015 (M_w6.5) mainshocks. This methodology has been widely used globally (e.g., Akinci et al., 2017; Graves & Pitarka, 2004; Mena et al., 2010; Pischiutta et al., 2020) but little work has been performed in Greece (e.g., Kiratzi et al., 2019; Roumelioti et al., 2016). For frequencies higher than 1.5 Hz, where source and wave propagation effects become stochastic, a finite fault simulation model based on a dynamic corner frequency was applied via the EXSIM code. For the LF part of the synthetic seismograms, a deterministic method was employed through COMPSYN, a well-established code to calculate synthetic time series occurring on extended faults by computing Green's functions using the Discrete Wavenumber/Finite Element (DWFE) method of Olson et al. (1984). The results from each simulation method were eventually merged in the frequency domain using the technique of Mai and Beroza (2003).

The spatial distribution of the simulated ground motions, in the near-field, in terms of PGA and PGV (Figs. 5, 6) reveals that they are highly influenced by the slip heterogeneity within the seismic source. The ground motion amplification pattern depends on the relative location of the large slip patches that produce larger ground motion above the large slip areas. Site specific simulated PGA values show good correlation with the maximum recorded PGA values and the acceleration maps are supported by macroseismic and other observations. Small discrepancies are observed in sites such as the LXRB station, which is located on the surface projection of the activated fault. In general, the simulated PGA values show good agreement

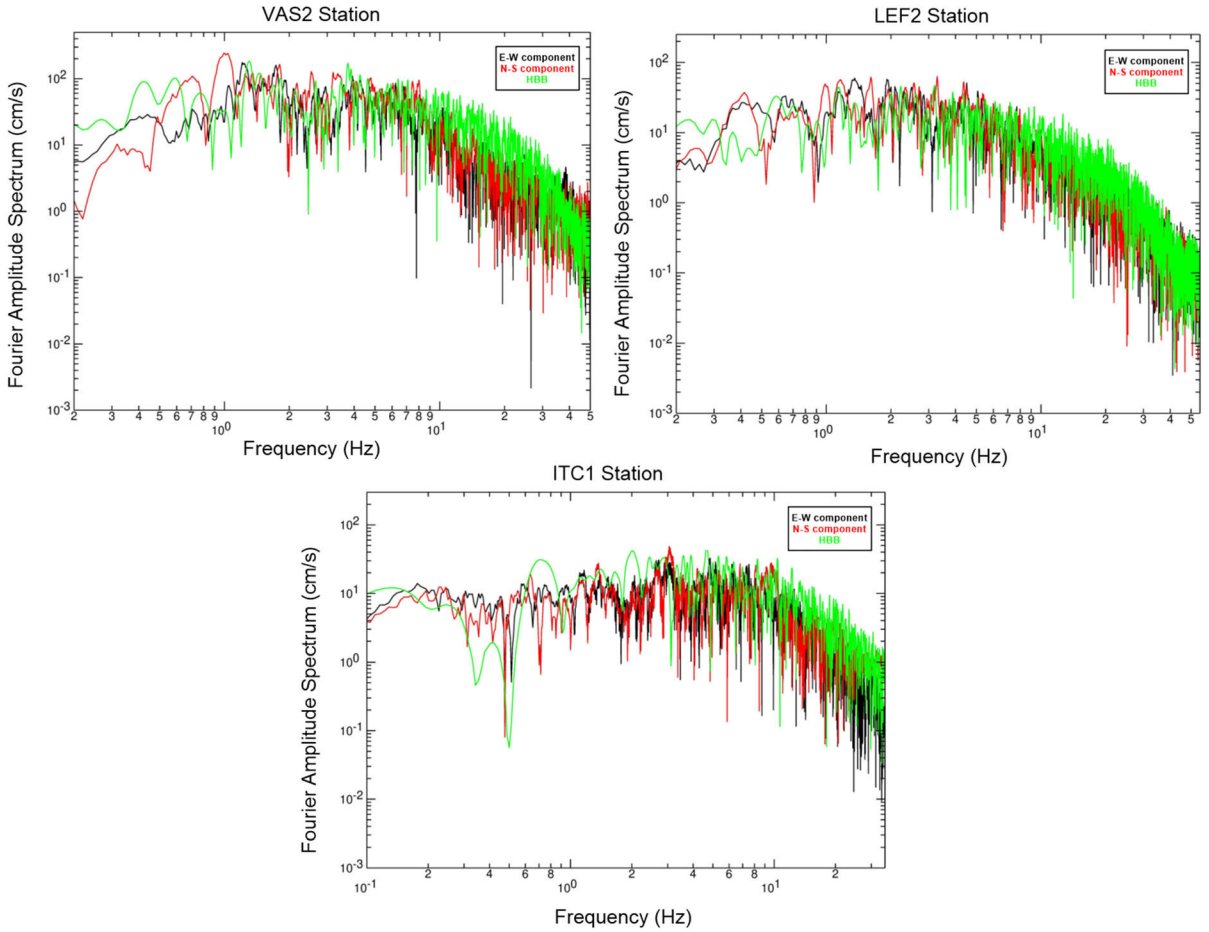

Figure 11
Fourier amplitude spectra for the November 17th M_w6.5 Lefkas earthquake at four selected stations (red and black lines correspond to N-S and E-W components respectively) in comparison with the simulated ground motions (green lines) obtained using the hybrid approach

with the values computed by the GMPEs especially as R_{jb} increases (Figs. 7, 8). The comparison of the synthetic with the recorded FAS revealed a satisfactory fit both in amplitude and envelope shapes (Figs. 9, 11), despite the fact that ground motions in some stations are slightly overestimated (VAS2 station) or underestimated (LXRB station). As far as the synthetic waveforms are concerned, the general shape and duration seem to be sufficiently represented by the hybrid simulations (Figs. 10, 12).

During the course of this study, the role of various fundamental seismological source and path parameters was investigated leading to a series of remarks. Firstly, PGA variations were strongly influenced by slip heterogeneities and changes in the rupture propagation, such as the fault edges. PGA levels are primarily controlled by the focal depth, the assumed rupture velocity and the average stress drop. The average stress drop effect seems to gradually decrease in the far-field making room for other path and site related parameters. It should be also noted that the slip distribution model does not considerably control the average simulated PGA values, yet it significantly contributes to the strong ground motion variability in the near-field.

Useful applications can be performed based on the results of the present study as well as plenty of possibilities for future research. Firstly, the applied methodology can be used in order to simulate past strong earthquakes, for which there are no available

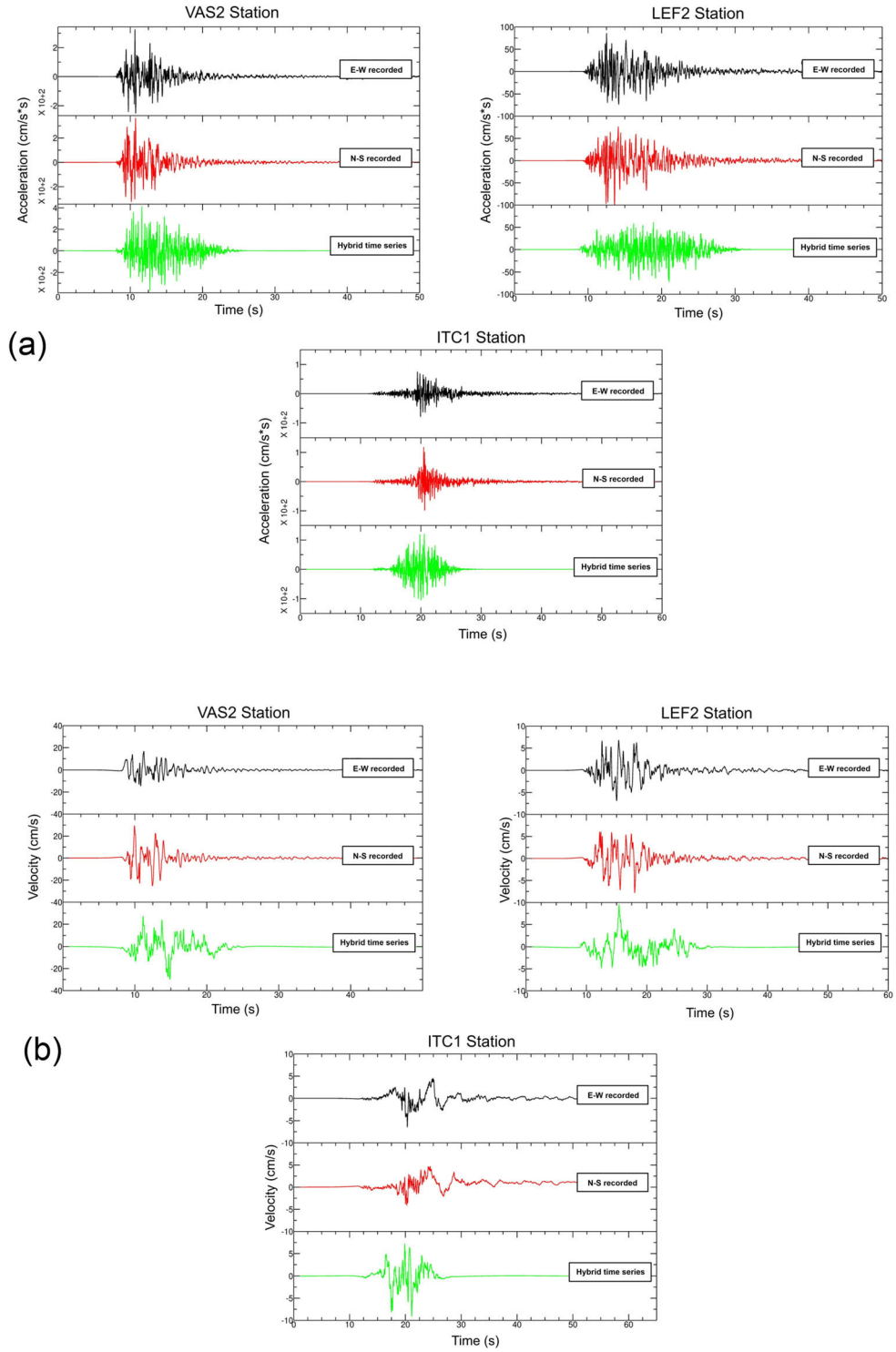

Figure 12
Comparison between recorded (red and black) and synthetic (green) broadband **a** acceleration and **b** velocity time series for the three selected stations for the November 17th $\mathbf{M_w 6.5}$ Lefkas earthquake

Table 2

Empirical attenuation factors for soil type B adopted by Margaris and Boore (1998)

f (Hz)	Amplification
0.01	1.00
0.09	1.21
0.16	1.32
0.51	1.59
0.84	1.77
1.25	1.96
2.26	2.25
3.17	2.42
6.05	2.70
16.6	3.25
61.2	4.15

recordings. In this manner, a potential strong ground motion database for a time period much longer than the recent instrumental period can be created and used in multiple applications, such as the development of a region specific GMPE. The main challenge that modern GMPEs face is their inability to estimate strong ground motion in the near-field due to the lack of strong motion recordings and their inadequacy in replicating the directivity effects which are commonly observed in the near-field. The innovation introduced in the present and similar studies will lead to the development of reliable GMPEs that can reflect the near-source and directivity effects, contrary to the ones used in the past and nowadays.

Due to the increased level of complexity of the scientific topics undertaken in this study, the research was based on several limitations and assumptions. The uniform type B soil condition considered for the calculations in the study area is a case in point. This assumption was necessary for two reasons; the first one was the inability of COMPSYN to adequately incorporate the local site effects and the second was the lack of sufficient and/or reliable site characterization data for the study area. Consequently, the results of the present study can be improved in the future by taking into consideration the local site condition variability, for example by using Vs_{30} profiles covering the entire study area or by using ambient noise (HVSR), a technique widely used in Greece for site effects characterization (e.g., Apostolidis, 2002; Kassaras et al., 2015; Leventakis, 2003; Panou et al., 2005; Triantafyllidis et al., 2006).

The present study could be extended to generate synthetic ground motions for future strong earthquakes via a "most-probable" or a "worst-case" scenario. This complex procedure requires the definition of the magnitude and the rupture area, the examination of multiple hypothetical nucleation points and the resulting slip distribution, which can be represented by either kinematic or more complex dynamic rupture models. The results of this analysis could ultimately be compared to probabilistic seismic hazard maps in order to assess the level of expected PGA. It is worth stating that, in the framework of the present study, only a one-dimensional velocity model is considered to generate synthetic ground motion together with a stochastic method. Accounting for the 3D velocity model throughout the deterministic approaches may improve ground motion results including the structural complexity of sedimentary basin and the surface topography effects.

Acknowledgements

The authors would like to thank Prof J. Julia for the editorial assistance and Dr S. Hok for the constructive and detailed comments that contributed to the significant improvement of the manuscript. The authors declare that they have no conflicts of interest. Pavlos Bonatis (Geophysics Department, Aristotle University of Thessaloniki) was at the INGV in Rome, Italy, supported by the Erasmus + traineeship grant when a substantial part of this study was conducted. The seismicity data were provided by the bulletins of the Seismological Station of the Aristotle University of Thessaloniki (http://seismology.geo.auth.gr/ss/). Acceleration time histories were provided by ITSAK (Institute of Earthquake Engineering and Engineering Seismology; http://www.itsak.gr) and NOA (National Observatory of Athens; http://bbnet.gein.noa.gr/HL). Some figures were created using the Generic Mapping Tools version 4.5.3 (Wessel et al., 2013). Plots and some figures were created with Grapher version 10 (http://www.GoldenSoftware.com) The LF ground motion simulations were performed using COMPSYN sxv3.11

(Spudich & Xu, 2002). The HF ground motion simulations were carried out using the EXSIM_DMB code (http://www.daveboore.com/ software_online.html). Seismic signal analysis was performed using SAC (Seismic Analysis Code) version 101.6 (Goldstein et al., 2003; Goldstein & Snoke, 2005). Geophysics Department Contribution 952.

Publisher's Note Springer Nature remains neutral with regard to jurisdictional claims in published maps and institutional affiliations.

References

Akinci, A., Aochi, H., Herrero, A., Pischiutta, M., & Karanikas, D. (2017). Physics-based broadband ground-motion simulations for probable Mw ≥7:0 earthquakes in the Marmara sea region (Turkey). *Bulletin of the Seismological Society of America, 107*, 1307–1323.

Akkar, S., & Bommer, J. (2010). Empirical equations for the prediction of PGA, PGV, and spectral accelerations in Europe, the Mediterranean region, and the middle east. *Seismological Research Letters, 81*, 195–206.

Anderson, J., & Hough, S. (1984). A model for the shape of the Fourier amplitude spectrum of acceleration at high frequencies. *Bulletin of the Seismological Society of America, 74*, 1969–1993.

Apostolidis, P. (2002). Determination of the soil structure using microtremors. Application to the estimation of the dynamic properties and the geometry of the soil formations at Thessaloniki city. PhD Thesis (in Greek), Aristotle University of Thessaloniki, 315 p

Assatourians, K., Atkinson, G. (2012). EXSIM12: a Stochastic Finite- Fault Computer Program in FORTRAN. http://www.seismotoolbox.ca (last accessed November 2014)

Avallone, A., Cirella, A., Cheloni, D., Tolomei, C., Theodoulidis, N., Piatanesi, A., Briole, P., & Ganas, A. (2017). Near-source high-rate GPS, strong motion and InSAR observations to image the 2015 Lefkada (Greece) Earthquake rupture history. *Scientific Reports, 7*, 10358.

Boore, D. (1983). Stochastic simulation of high-frequency ground motions based on seismological models of the radiated spectra. *Bulletin of the Seismological Society of America, 73*, 1865–1894.

Boore, D. (2003). Prediction of ground motion using the stochastic method. *Pure and Applied Geophysics, 160*, 635–676.

Boore, D. M. (2009). Comparing stochastic point-source and finite-source ground-motion simulations: SMSIM and EXSIM. *Bulletin of the Seismological Society of America, 99*(6), 3202–3216.

Boore, D. M., Stewart, J. P., Seyhan, E., & Atkinson, G. M. (2014). NGA-West2 equations for predicting PGA, PGV, and 5% damped PSA for shallow crustal earthquakes. *Earthquake Spectra, 30*(3), 1057–1085.

Boore, D. M., Stewart, J. P., Skarlatoudis, A. A., Seyhan, E., Margaris, B., Theodoulidis, N., Scordilis, E., Kalogeras, I., Klimis, N., & Melis, N. S. (2020). A Ground-motion prediction model for shallow crustal earthquakes in Greece. *Bulletin of the Seismological Society of America, 111*(2), 857–874.

Chousianitis, K., Konca, A. O., Tselentis, G.-A., Papadopoulos, G., & Gianniou, M. (2016). Slip model of the 17 November 2015 Mw = 6.5 Lefkada earthquake from the joint inversion of geodetic and seismic data. *Geophysical Research Letters, 43*, 7973–7981.

Clément, C., Hirn, A., Charvis, P., Sachpazi, M., & Marnelis, F. (2000). Seismic structure and the active Hellenic subduction in the Ionian Islands. *Tectonophysics, 329*, 141–156.

Ding, Y., Mavroeidis, G., & Theodoulidis, N. (2019). Simulation of strong ground motion from the 1995 Mw 6.5 Kozani-Grevena, Greece, earthquake using a hybrid deterministic-stochastic approach. *Soil Dynamics and Earthquake Engineering, 117*, 357–373.

Douglas, J., & Aochi, H. (2008). A survey of techniques for predicting earthquake ground motions for engineering purposes. *Surveys in Geophysics, 29*, 187–220.

Ganas, A., Elias, P., Bozionelos, G., Papathanassiou, G., Avallone, A., Papastergios, A., Valkaniotis, S., Parcharidis, I., & Briole, P. (2016). Coseismic deformation, field observations and seismic fault of the 17 November 2015 M = 6.5, Lefkada Island, Greece Earthquake. *Tectonics, 687*, 210–222.

Gardner, G., Gardner, W., & Gregory, R. (1974). Formation velocity and density—the diagnostic basics for stratigraphic traps. *Geophysics, 39*, 770–780.

Goldstein, P., Dodge, D., Firpo, M., and Minner, L. (2003). "SAC2000: Signal processing and analysis tools for seismologists and engineers, Invited contribution to *"The IASPEI International Handbook of Earthquake and Engineering Seismology"*, Edited by WHK Lee, H. Kanamori, P.C. Jennings, and C. Kisslinger, Academic Press

Goldstein, P., Snoke, A. (2005). "SAC Availability for the IRIS Community", Incorporated Institutions for Seismology Data Management Center Electronic Newsletter

Graves, R. and Pitarka, A. (2004). Broadband time history simulation using a hybrid approach. *Proceedings of the 13th World Conference on Earthquake Engineering*, Paper no. 1098

Graves, R., & Pitarka, A. (2010). Broadband ground-motion simulation using a hybrid approach. *Bulletin of the Seismological Society of America, 100*(5A), 2095–2123.

Hartzell, H. (1978). Earthquake aftershocks as Green's functions. *Geophysical Research Letters, 5*, 1–4.

Hatzidimitriou, P. (1995). S-wave attenuation in the crust in Northern Greece. *Bulletin of the Seismological Society of America, 85*, 1381–1387.

Hatzidimitriou, P., Papazachos, C., Kiratzi, A., & Theodulidis, N. (1993). Estimation of attenuation structure and local earthquake magnitude based on acceleration records in Greece. *Tectonophysics, 217*, 243–253.

Irikura, K. (1986). Prediction of strong acceleration motion using empirical Green's function. *Proceedings of the 7th Japan Earthquake Engineering Symposium*, 151–156

Irikura, K., & Miyake, H. (2011). Recipe for predicting strong ground motion from crustal earthquake scenarios. *Pure and Applied Geophysics, 168*, 85–104.

Kanamori, H., & Anderson, D. (1975). Theoretical basis of some empirical relations in seismology. *Bulletin of the Seismological Society of America, 65*, 1073–1095.

Karakostas, V., Papadimitriou, E., Mesimeri, M., Gkarlaouni, C., & Paradisopoulou, P. (2015). The 2014 Kefalonia doublet (M w 6.1

and M w 6.0), central Ionian islands, Greece: seismotectonic implications along the Kefalonia transform fault zone. *Acta Geophysica, 63*, 1–16.

Karakostas, V., Papadimitriou, E., & Papazachos, C. (2004). Properties of the 2003 Lefkada, Ionian islands, Greece, Earthquake seismic sequence and seismicity triggering. *Bulletin of the Seismological Society of America, 94*(5), 1976–1981.

Karastathis, V., Mouzakiotis, A., Ganas, A., & Papadopoulos, G. (2015). High-precision relocation of seismic sequences above a dipping Moho: the case of the January–February 2014 seismic sequence on Cephalonia Island (Greece). *Solid Earth, 6*, 173.

Kassaras, I., Kalantoni, D., Benetatos, Ch., Kaviris, G., Michalaki, K., Sakellariou, N., & Makropoulos, K. (2015). Seismic damage scenarios in Lefkas old town (W. Greece). *Bulletin of Earthquake Engineering, 13*, 3669–3711.

Kiratzi, A., & Langston, C. (1991). Moment tensor inversion of the 1983 January 17 Kefallinia event of Ionian islands (Greece). *Geophysical Journal International, 105*, 529–538.

Kiratzi, A., Roumelioti, Z., Makra, K., Klimis, N., and Koskosidi, A. (2019). Hybrid broadband seismic ground motions: application to the city of Edessa in northern Greece. *7th International Conference on Earthquake Geotechnical Engineering (VII ICEGE), 17–20 June 2019*

Klimis, N., Margaris, B., & Koliopoulos, P. (1999). Site dependent amplification functions and response spectra in Greece. *Journal of Earthquake Engineering, 3*(2), 237–247.

Leventakis, A. (2003). Microzonation study of the city of Thessaloniki, PhD, Aristotle University of Thessaloniki, 84 p

Louvari, E., Kiratzi, A. A., & Papazachos, B. C. (1999). The Cephalonia transform Fault and its extension to western Lefkada Island (Greece). *Tectonophysics, 308*, 223–236.

Mai, P. M. (2009). Ground motion: complexity and scaling in the near field of earthquake ruptures, *Encyclopedia of Complexity and Systems Science*, Springer, 4435–4474

Mai, M., & Beroza, C. (2003). A hybrid method for calculating nearsource, broadband seismograms: application to strong motion prediction. *Physics of the Earth and Planetary Interiors, 137*(1), 183–199.

Makropoulos, K., Kaviris, G., & Kouskouna, V. (2012). An updated and extended earthquake catalogue for Greece and adjacent areas since 1900. *Natural Hazards and Earth System Sciences, 12*, 1425–1430.

Margaris, B. N., & Boore, D. M. (1998). Determination of $\Delta\sigma$ and $\kappa 0$ from response spectra of large earthquakes in Greece. *Bulletin of the Seismological Society of America, 88*, 170–182.

Margaris, B., & Hatzidimitriou, P. (2002). Source spectral scaling and stress release estimates using strong-motion records in Greece. *Bulletin of the Seismological Society of America, 92*, 1040–1059.

McKenzie, D. (1978). Some remarks on the development of sedimentary basins. *Earth and Planetary Science Letters, 40*, 25–32.

Mena, B., Mai, P., Olsen, K., Purvance, M., & Brune, J. (2010). Hybrid broadband ground-motion simulation using scattering Green's functions: application to large-magnitude events. *Bulletin of the Seismological Society of America, 100*, 2143–2162.

Millas, Ch. (2018). Slip distribution of large earthquakes In Greece, MSc Thesis, National and Kapodistrian University of Athens, 74p

Millas, Ch., Kaviris, G., Karakostas, V., and Papadimitriou, P. (2018). Slip distribution and resulting surface deformation assessment of strong earthquakes in Greece. Abstract, *36th ESC General Assembly*, ESC2018-S19-573

Motazedian, D., & Atkinson, G. M. (2005). Stochastic finite-fault modeling based on a dynamic corner frequency. *Bulletin of the Seismological Society of America, 95*, 995–1010.

Mouzakiotis, E. (2015). Seismic hazard assessment using the method of stochastic simulation of strong ground motion, MSc Thesis, National and Kapodistrian University of Athens, 155p

Olson, A., Orcutt, J., & Frazier, G. (1984). The discrete wavenumber / finite element method for synthetic seismograms. *Geophysical Journal of the Royal Astronomical Society, 77*, 421–460.

Panou, A., Theodoulidis, N., Hatzidimitriou, P., Stylianidis, K., & Papazachos, C. (2005). Ambient noise horizontal-to-vertical spectral ratio in site effects estimation and correlation with seismic damage distribution in urban environment: the case of the city of Thessaloniki (Northern Greece). *Soil Dynamics and Earthquake Engineering, 25*, 261–274.

Papadimitriou, E. (2002). Mode of strong earthquake recurrence in the central Ionian Islands (Greece): possible triggering due to Coulomb stress changes generated by the occurrence of previous strong shocks. *Bulletin of the Seismological Society of America, 92*(8), 3293–3308.

Papadimitriou, E., Karakostas, V., Mesimeri, M., Chouliaras, G., & Kourouklas, Ch. (2017). The Mw6.5 17 November 2015 Lefkada (Greece) earthquake: structural interpretation by means of the aftershock analysis. *Pure and Applied Geophysics, 174*, 3869–3888.

Papadimitriou, P. (1988). Etude de la structure du manteau superieur de l' Europe et modelisation des ondes de volume engendrees par des seismes Egeens. Phd Thesis, University Paris, 211p

Papadimitriou, P., Karakonstantis, A., Bozionelos, G., Kapetanidis, V., Kaviris, G., Spingos, I., Millas, Ch., Kassaras, I., and Voulgaris, N. (2015). Preliminary report on the Lefkada 17 November 2015 Mw=6.4 earthquake, 12p

Papadopoulos, G., Karastathis, V., Koukouvelas, I., Sachpazi, M., Baskoutas, I., Chouliaras, G., Agalos, A., Daskalaki, E., Minadakis, G., Moshou, A., Mouzakiotis, A., Orfanogiannaki, K., Papageorgiou, A., Spanos, D., and Triantafyllou, I. (2014). The Cephalonia, Ionian Sea (Greece), sequence of strong earthquakes of January-February 2014: a first report. *Research in Geophysics*, 4(1).

Papathanassiou, G., Valkaniotis, S., Ganas, A., Grendas, N., & Kollia, E. (2017). The November 17th, 2015 Lefkada (Greece) strike-slip earthquake: field mapping of generated failures and assessment of macroseismic intensity ESI-07. *Engineering Geology, 220*, 13–30.

Papazachos, B., & Comninakis, P. (1969). 1970, Geophysical features of the Greek Island Arc and Eastern Mediterranean ridge. *Comptes Rendus Des Seances De La Conference Reunie a Madrid, 16*, 74–75.

Papazachos, B. C., Papadimitriou, E., Kiratzi, A., Papazachos, C. B., & Louvari, E. (1998). Fault plane solutions in the Aegean sea and the surrounding area and their tectonic implication. *Bolletino Di Geofisica Teorica Ed Applicata, 39*(3), 199–218.

Papazachos, B. C., & Papazachou, C. B. (2003). *The earthquakes of Greece* (p. 273). Ziti publications.

Pischiutta, M., Akinci, A., Tinti, E., & Herrero, A. (2020). Broadband ground-motion simulation of 2016 Amatrice

earthquake Central Italy. *Geophysical Journal International*. https://doi.org/10.1093/gji/ggaa412

Pitarka, A., Graves, R., Irikura, K., Miyakoshi, K., & Rodgers, A. (2020). Kinematic rupture modeling of ground motion from the M7 Kumamoto, Japan earthquake. *Pure and Applied Geophysics, 177*, 2199–2221.

Rodgers, A. J., Pitarka, A., Petersson, N. A., Sjogreen, B., & McCallen, D. (2018). Broadband (0–4 Hz) ground motions for a magnitude 7.0 Hayward Fault earthquake with 3D structure and topography. *Geophysical Research Letters, 45*, 739–747.

Roumelioti, Z., Kiratzi, A., Margaris, B., & Chatzipetros, A. (2016). Simulation of strong ground motion on near-fault rock outcrop for engineering purposes: the case of the city of Xanthi (Northern Greece). *Bulletin of Earthquake Engineering, 15*, 25–49.

Scordilis, M., Karakaisis, G., Karakostas, V., Panagiotopoulos, D. G., Comninakis, P. E., & Papazachos, B. C. (1985). Evidence for transform faulting in the Ionian sea: the Cephalonia island earthquake sequence of 1983. *Pure and Applied Geophysics, 123*, 388–397.

Sokos, E., Kiratzi, A., Gallovič, F., Zahradnik, J., Serpetsidaki, A., Plicka, V., Janský, J., Kostelecký, J., & Tselentis, A. (2015). Rupture process of the 2014 Cephalonia, Greece, earthquake doublet (Mw6) as inferred from regional and local seismic data. *Tectonophysics, 656*, 131–141.

Sokos, E., Zahradník, J., Gallovič, F., Serpetsidaki, A., Plicka, V., & Kiratzi, A. (2016). Asperity break after 12 years: the Mw6.4 2015 Lefkada (Greece) earthquake. *Geophysical Research Letters, 43*, 6137–6145.

Spudich, P., & Archuleta, R. (1987). Techniques for earthquake ground motion calculation with applications to source parameterization of finite faults. *Seismic Strong Motion Synthetics, 37*, 205–265.

Spudich, P., Xu, L. (2002) Documentation of Software Package Compsyn sxv3.11: programs for earthquake ground motion calculation using complete 1-D Green's functions. *International Handbook of Earthquake and Engineering Seismology*, 1200p

Theodoulidis, N., Karakostas, C., Lekidis, V., Makra, K., Margaris, B., Morfidis, K., Papaioannou, Ch., Rovithis, E., Salonikios, T., & Savvaidis, A. (2016). The Cephalonia, Greece, January 26 (M6.1) and February 3, 2014 (M6.0) earthquakes: near-fault ground motion and effects on soil and structures. *Bulletin of Earthquake Engineering, 14*, 1–38.

Triantafyllidis, P., Theodulidis, N., Savvaidis, A., and Dimitriou, P. (2006) Site effects estimation using earthquake and ambient noise data: the case of Lefkas town. *Proceedings of the First European conference on earthquake engineering and seismology. Geneva, 3–8 Sept 2006*, paper no. 1249

Valkaniotis, S., Ganas, A., Papathanassiou, G., & Papanikolaou, M. (2014). Field observations of geological effects triggered by the January-February 2014 Cephalonia (Ionian Sea, Greece) earthquakes. *Tectonophysics, 630*, 150–157.

Wessel, P., Smith, W. H. F., Scharroo, R., Luis, J., & Wobbe, F. (2013). Generic mapping tools: improved version released. *EOS Transactions, 94*(45), 409–410.

Withers, K., Olsen, K., Day, S., & Shi, Z. (2018). ground motion and intraevent variability from 3D deterministic Broad530 band (0–7.5 Hz) simulations along a nonplanar strike-slip fault. *Bulletin of the Seismological Society of America, 109*, 229–250.

Zahradnik, J., Sokos, E. (2015). Lefkada 17/11/2015, Mw 6.4 event: Quick estimate of source complexity. Report sent to EMSC on 22/11/2015, 11p

(Received October 21, 2020, revised July 8, 2021, accepted July 11, 2021)